ELSEVIER

Nuclear Physics A 601 (1996) 1–40

NUCLEAR PHYSICS A

Particle–hole and particle–particle correlations in neodymium isotopes

V.Yu. Ponomarev [a,c], M. Pignanelli [a,1], N. Blasi [a], A. Bontempi [a], J.A. Bordewijk [b], R. De Leo [d], G. Graw [e], M.N. Harakeh [b], D. Hofer [e], M.A. Hofstee [b], S. Micheletti [a], R. Perrino [f], S.Y. van der Werf [b]

[a] *Dipartimento di Fisica dell'Università and Sezione INFN, via Celoria 16, I-20133 Milano, Italy*

[b] *Kernfysisch Versneller Instituut, Zernikelaan 25, 9747 AA Groningen, The Netherlands*

[c] *Laboratory of Theoretical Physics, Joint Institute for Nuclear Research, Dubna, Head Post Office, P.O. Box 79, Moscow, Russian Federation*

[d] *Dipartimento di Fisica dell'Università and Sezione INFN, via Amendola 173, I-70126 Bari, Italy*

[e] *Sektion Physik der Universität München, 85748 Garching, Germany*

[f] *Sezione INFN, via Arnesano, I-73100 Lecce, Italy*

Received 22 March 1995; revised 8 December 1995

Abstract

Excited states in ^{140,142,144,146}Nd nuclei, up to an excitation energy of about 5 MeV, were investigated by (p,t) experiments performed with a good energy resolution. These data, together with proton and deuteron scattering data from a previous experiment, are compared with Quasi-Particle Phonon Model evaluations, in which the competition between particle–hole and particle–particle residual interactions is considered. The $B(E\lambda)$ distributions are satisfactorily reproduced. The ^{146,148}Nd(p,t) reaction data are well accounted for, while difficulties are found in reproducing those for ^{142,144}Nd(p,t). Limitations and improvements of the model are discussed.

PACS: 21.10.Jx; 21.60.Jz; 25.40.Jt; 27.60.+j

Keywords: NUCLEAR REACTIONS ^{142,144,146}Nd(p,t), E = 35.6 MeV; ^{148}Nd(p,t), E = 25 MeV; measured $\sigma(\theta)$. ^{140,142,144,146}Nd deduced levels; J, π; enriched targets; comparison with microscopic calculations

1. Introduction

Particle–hole (p–h) and particle–particle (p–p) correlations play a fundamental role in the structure of nuclei. The first type of correlations gives rise to the well-established

[1] Corresponding author.

SSDI 0375-9474(95)00504-8

rotational and vibrational modes, which are strongly excited in inelastic processes. The p–p or h–h correlations affect particles moving around the Fermi surface and produce vibrations, which change the number of particles by two (pair vibrations [1,2]). The last correlations can be generated by a two-body interaction: the pairing field. A reaction in which two particles are transferred to a nucleus in an $L = 0$, $S = 0$, $T = 1$ state is a specific probe of pair correlations. This situation is experimentally realized with (t,p) and (p,t) reactions. Since the transfer of a dineutron can be expressed in terms of the pairing field, it is natural to analyze two-neutron transfer reactions with the help of these fields and conversely, the (p,t) and (t,p) reactions make it possible to study the pair correlations and to explore the dynamical effects of the pairing fields.

In the present study the excited states in ^{140,142,144,146}Nd, up to excitation energies of about 5 MeV, have been investigated by the (p,t) reaction. The (p,t) cross sections have been analyzed together with reduced transition probabilities from a previous study of proton and deuteron scattering on even Nd isotopes [3]. In this latter study the experimental strength distributions were compared with the predictions of the Interacting Boson Model (IBM [4]) and the Quasi-particle Phonon Model (QPM [5]). The latter is a microscopic model in which the basis states, called "phonons", are the collective and non-collective solutions of the BCS quasi-particle RPA equations. In the QPM evaluations, two- and three-phonon states are constructed and simultaneously coupled and mixed. The fact that this model takes into account not only the strong collective configurations but also states with a weaker collectivity down to quasi-particle states is of some interest in comparing with data that include also weak transitions. The model describes reasonably well [3] the isoscalar and isovector strength distributions for the different multipolarities from $\lambda = 2$ to 6.

The collective states, studied by inelastic scattering processes, gave information on p–h correlations in terms of a residual interaction. In a superfluid description p–h and p–p correlations should affect the same states [2]. For this reason in the present study we analyze simultaneously inelastic scattering and two-neutron transfer reactions. In particular, the B(E2) value and the (p,t) cross section for the excitation of the first 2^+ state are used to obtain information on the quadrupole pairing force.

2. The experimental method and results

In a previous experiment, described in Ref. [3], the differential inelastic cross sections for proton and deuteron scattering on ^{142,144,146,148,150}Nd have been measured. The incident energies were 30.5 and 50.8 MeV, respectively, for protons and deuterons. The energy resolution was 12–15 keV in (p,p′) and 15–22 keV in (d,d′) experiments. The weakest transitions detected in inelastic scattering experiments have differential (p,p′) cross sections reaching, at the maximum in the angular distribution, a value of the order of 15–20 μb/sr. These cross sections correspond, for a transition to a 2^+ state, to a B(E2) value of 0.1 single particle Weisskopf unit (spu).

The (p,t) reaction on Nd isotopes was studied already more than 20 years ago: on

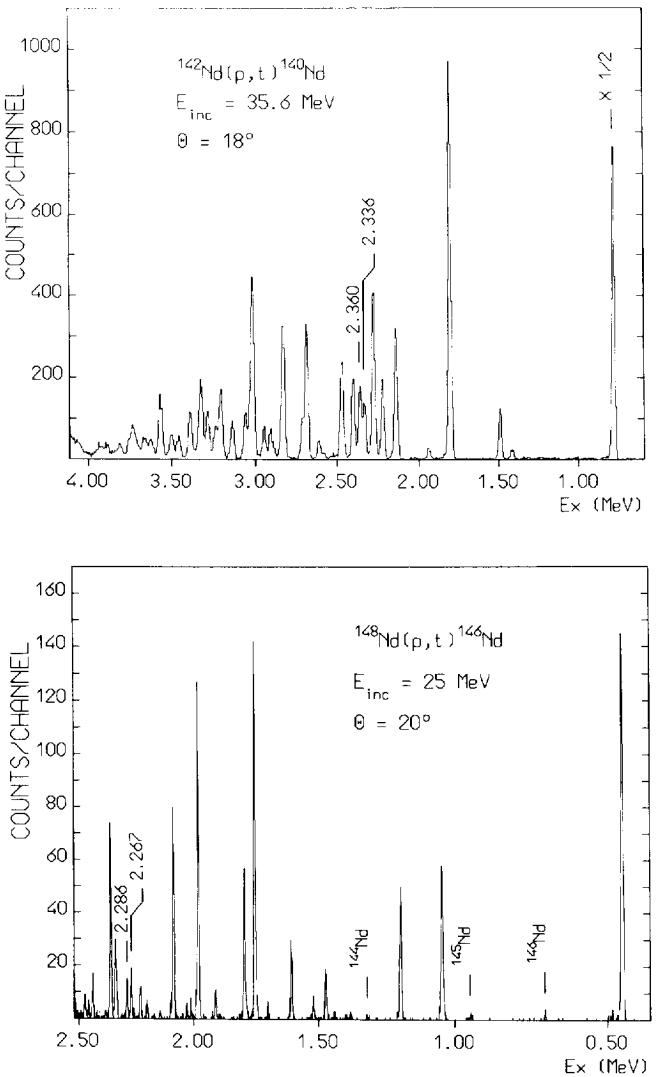

Fig. 1. Triton spectra from ^{142}Nd(p,t) and ^{148}Nd(p,t) reactions, observed at two different incident energies and with a different resolving power.

^{142,144,146}Nd at an incident energy of 31 MeV, with an energy resolution of 20 keV by Ball et al. [6] and at 52 MeV on the whole family of even Nd isotopes by Yagi et al. [7]. Unfortunately, in the first experiment only the strong transitions were studied, while the second experiment was performed with an energy resolution of 80 keV. In the present study the ^{142,144,146}Nd(p,t) reactions have been studied using a momentum-analyzed beam of 35.6 MeV from the KVI cyclotron. The tritons were detected in the focal plane of the QMG/2 spectrograph with an energy resolution of 20–25 keV. The ^{148}Nd(p,t) reaction has been studied using a 25 MeV proton beam from the Munich MP tandem accelerator, with an energy resolution of 7–9 keV. Triton spectra, measured at

Table 1
Proton incident energies, highest measured excitation energies (E_{max}), target thickness, isotopic enrichment, angular range and step for the various reactions

Reaction	E_p (MeV)	E_{max} (MeV)	Thickness ($\mu g/cm^2$)	Enrichment (%)	$\theta_{min} - \theta_{max}$ (degree)	$\Delta\theta$ (degree)
^{142}Nd(p,t)	35.6	4.00	500	98.3	6–58	4
^{144}Nd(p,t)	35.6	4.90	500	97.5	6–58	4
^{146}Nd(p,t)	35.6	5.02	550	97.6	6–62	4
^{148}Nd(p,t)	25.0	5.00	57	96.6	5–60	5

the two incident energies, are shown in Fig. 1. The excitation energies were determined through the calibration of the focal plane detectors with known excitation energies. The accuracy of the method depends on the location of the calibration peaks and can, therefore, change for each target nucleus with the excitation energy. On average the energy values quoted in the present paper have an uncertainty of about 2 keV for the states below E_x = 2.5 MeV and a larger uncertainty, increasing up to 5–7 keV, at the highest energies, due to the lack of good reference levels.

Targets, enriched to about 98 (96)% and with a thickness of about 500 (60) $\mu g/cm^2$ have been used in KVI (Munich) experiments. Triton energy spectra have been measured up to the excitation energies and at the angles given in Table 1. The cross section for each peak was obtained from its area using the quoted target thickness, the solid angle ($\simeq$ 5 msr) and the collected charge. The weakest transitions observed have, at the maximum in the angular distribution, a cross section of 2–3 $\mu b/sr$ in the KVI experiments and of 1–2 $\mu b/sr$ in the Munich experiment. Proton elastic scattering cross sections for each nucleus have been measured and compared to optical model predictions in order to test the accuracy in determining the absolute cross section values. The accuracy in the cross section normalization has been estimated to be of the order of 5–10% in the case of ^{142,144,146}Nd targets and of 10–15% for ^{148}Nd. The relative values of the cross sections, for different transitions from the same target nucleus, should have a better accuracy.

The cross section values, obtained at θ_{Lab} = 10°, and their errors are given in Tables 2–5. To compare the experiment to model predictions, the cross section value (σ_{max}) at the main maximum of the angular distribution has been considered. In the case of angular distributions with scattered points and where the maximum is located at 0°, σ_{max} has been obtained with the help of DWBA curves to interpolate or extrapolate the data. The errors in σ_{max} values have been estimated from the uncertainties of the normalization of the DWBA curves to the experimental data.

About 350 (p,t) transitions to final states of the ^{140,142,144,146}Nd isotopes have been studied. Several states, not reported in the literature [8–11], have been detected and their spin-parity has been assigned by the analysis described in the next section. The excitation energy and the spin-parity of the states of the different nuclei as deduced from the present and previous studies are given in Tables 2–5. These tables are of some interest in connection with the fact that a large body of data is required to test nuclear structure models. The importance of reactions that provide "complete spectroscopy" has

Table 2
Spectroscopic information on ^{140}Nd available in literature and deduced from the present experiment. In the last two columns the (p,t) cross sections $\sigma(10°)$ at the center mass angle of 10.1°, and those at the main maximum in the angular distribution, σ_{max}, are given. The numbers in round brackets are the statistical errors and the uncertainties in the normalization of the DWBA curves to the experimental angular distributions in the case of $\sigma(10°)$ and of σ_{max}, respectively

Ref. [8]		Present experiment			
E_x (MeV)	J^π	E_x (MeV)	J^π	$\sigma(10°)$ (μb/sr)	σ_{max} (μb/sr)
0.000	0^+	0.000	0^+	574(5)	700(70)
0.7737	2^+	0.774	2^+	829(8)	1300(65)
1.4132	0^+	1.414	2^+	9(0.8)	50 [a](15)
1.4900	(2^+)	1.490	(2^+)	67(2)	100(10)
1.8019	4^+	1.802	4^+	201(4)	250(13)
		1.936	3^-	7.3(0.7)	30 [a](9)
2.1240	(3^-)				
2.1403	$(0,1,2)^+$	2.140	2^+	166(3)	210(11)
2.2215	7^-	2.224	7^-	48(2)	115(6)
2.2761	5^-	2.276	5^-	78(2)	160(16)
2.330	0^+				
2.3324	$(1^+,2^+)$	2.336	2^+	77(2)	120(12)
		2.360	0^+	78(2)	108(16)
2.3664	6^+				
		2.400	4^+	44(2)	55(6)
		2.468	2^+	140(3)	200(10)
		2.514	5^-	3(0.5)	3.3(0.5)
2.5477	$0^+(1,2)^-$	2.550	(0^+)	4.7(0.6)	11(1.7)
		2.575	$(4^+,5^-)$	1.7(0.3)	3.3(0.3)
		2.606	3^-	20(1.5)	20(1)
		2.686	4^+	61(2)	90(5)
		2.710	2^+	37(2)	60(9)
		2.830	(2^+)	123(3)	122(24)
2.8422	$(6,7)^-$				
		2.889	(5^-)	3.5(0.7)	4.5(0.7)
		2.911	0^+	32(2)	50(5)
2.9436	6^+	2.945	(6^+)	25(1.5)	20(4)
		3.014	4^+	88(2.5)	125(6)
		3.061	4^+	18(1)	28(3)
3.0618	7^-				
		3.136	(4^+)	30(1.5)	30(6)
		3.206	(2^+)	66(2)	90(9)
		3.239	(2^+)	18(1.5)	40(6)
		3.286	4^+	18(1.5)	30(3)
		3.324	$2^+ + 4^+$	59(2)	40(8)+30(6)
		3.387	2^+	48(2)	80(12)
		3.460	4^+	14(1.1)	16(2)
		3.494	4^+	15(1.2)	16(3)
		3.510		8(1)	8(1.4)
		3.561	(2^+)	38(1.7)	60(9)
		3.574	3^-	21(1.4)	26(3)
		3.621	(4^+)	7.2(1)	12(2)

Table 2 — continued

Ref. [8]		Present experiment			
E_x (MeV)	J^π	E_x (MeV)	J^π	$\sigma(10°)$ (μb/sr)	σ_{max} (μb/sr)
3.6733	7^-	3.666	(7^-)	7(1)	16(2)
		3.733		18(1)	15(3)
		3.755	6^+	7.8(1)	20(2)
		3.810		12(1.3)	20(4)
		3.844	(6^+)	5(1)	7(1.5)
		3.889	(1^-)	21(1)	45(5)
		3.925		6.8(1)	7(1.4)
		3.949		2(1.4)	6(1.2)

[a] Corrected for two-step contributions.

been discussed also recently by several authors. It has been shown, for instance, that neutron capture and fusion reactions have completeness properties [12]. By contrast, the (p,t) reaction is generally considered an inherently selective process, since it populates only neutron h–h configurations. For this reason the large number of transitions here observed is to some extent unexpected. The number of states in ^{144}Nd, lying at an excitation energy below 4 MeV and for which the spin-parity has been assigned is: 49 for states detected by (p,t) experiments, 38 by inelastic scattering and 23 by other reactions, as reported in Nuclear Data Sheets [10]. "Other reactions" include (n,γ), (n,n'γ), (light ion,xn), (HI,xnγ), one-nucleon transfer, beta decay, etc. Similarly in ^{146}Nd we have 88 states found in (p,t), 66 from (p,p') and 37 from other reactions [11]. The largest number of states has been, therefore, detected in (p,t) experiments. To explain this result it can be considered that

(1) the selectivity of the reaction results in a limited number of enhanced transitions, but if the experiment is performed using a magnetic spectrograph (large solid angle and high resolving power) also weak transitions are detected;

(2) the detection limit is mainly due to the peak to background ratio, that is particularly good in the case of (p,t) reactions;

(3) QPM calculations predict that most of the low-lying states have h–h components with a sizeable amplitude. Actually these evaluations predict a number of observable transitions of the same order of that experimentally detected. We like to stress here the fact that, in spite of its selectivity, the (p,t) reaction makes it possible to study also states that are hardly detected by other less selective reactions.

At high excitation (above 2.3, 4.1, 3.5 and 3.6 MeV for ^{140}Nd, ^{142}Nd, ^{144}Nd and ^{146}Nd, respectively) it is difficult to establish a direct correspondence between levels excited in this experiment and those seen in earlier reaction studies or in the recent inelastic scattering experiments [3]. This difficulty is due to several reasons:

(i) as noted above, the uncertainty in the level energies becomes larger;

(ii) most of the levels quoted in Nuclear Data Sheets at high energies are from γ-decay experiments in which the excitation energy is well determined, but the spin-parity, with the exception of few cases, is not assigned;

Table 3
Same as in Table 2 for ^{142}Nd. In columns 3 and 4, the information from recent (p,p′) and (d,d′) experiments [3] is also given

Ref. [9]		(p,p′), (d,d′) [a]		Present experiment			
E_x (MeV)	J^π	E_x (MeV)	J^π	E_x (MeV)	J^π	$\sigma(10°)$ (μb/sr)	σ_{max} (μb/sr)
0.000	0^+	0.000	0^+	0.000	0^+	504(5)	500(25)
1.5758	2^+	1.576	2^+	1.576	2^+	42(1)	90 [b](14)
2.0846	3^-	2.084	3^-	2.083	3^-	10(1)	40 [b](8)
2.1013	4^+	2.101	4^+	2.099	$(3^-,4^+)$	29(1)	22(3)
2.2098	6^+	2.209	$(4^+,6^+)$				
2.2172	0^+	2.217	0^+	2.217	0^+	25(1)	25(2.5)
		2.244	1^-				
2.3846	2^+	2.384	2^+	2.384	(2^+)	2.2(0.6)	1 [b](0.4)
2.4377	4^+	2.438	4^+	2.438	(4^+)	1.3(0.3)	1.8(0.4)
2.514	5^+	2.515	(1^-)				
				2.529		0.9(0.2)	3.5(0.5)
2.5478	3^+	2.549	(1^-)				
2.583	$1^{(+)}$	2.583	2^+	2.583	(1^+)	1.5(0.3)	2(0.3)
				2.656	0^+	1.6(0.3)	1.7(0.3)
2.7379	4^+	2.736	(4^+)				
		2.776	1^-	2.757	(1^-)	1.6(0.3)	3(0.6)
2.8459	2^+	2.846	2^+	2.846	(2^+)	9.2(0.7)	2 [b](0.8)
				2.873	(4^+)	2.5(0.4)	2.6(0.4)
2.8868	6^+	2.885	(6^+)				
				2.958	0^+	267(3)	280(10)
2.9597	4^-						
2.9766	(5^-)	2.975	5^-				
2.978	0^+			2.980	(0^+)	22(1)	20(2)
3.0096	$(\ )^-$	3.008	(3^-)	3.010	(3^-)	4.2(0.7)	5(0.7)
3.0457	(2^+)	3.045	2^+	3.046	(2^+)	1(0.6)	5 [b](2)
				3.078		1.1(0.6) 2(1)	
3.080		3.080	4^+				
3.1282	$(1,2^+)$	3.126	2^+				
				3.134	0^+	46(1.5)	50(5)
3.2431	7^-	3.241	7^-	3.242	7^-	2.2(0.4)	2.2(0.3)
3.2958	$(4)^-$	3.295	5^-	3.298	$(4^+,5^-)$	2.3(0.4)	2.8(0.4)
		3.315	4^+				
				3.319	1^-	4(0.5)	7(0.4)
3.3580	$(1,2)^+$						
		3.360	(5^-)	3.361	(5^-)	3.2(0.5)	3.3(0.4)
3.366	$(3)^-$						
3.413	5^-	3.408	$6^+(5^-)$	3.413	5^-	32(1.2)	35(1.7)
3.4249	1^-	3.420	1^-				
				3.469	2^+	389(4)	600(30)
3.4876	2^+						
		3.499	(7^-)				
		3.541	(7^-)				
3.574	$(3)^-$	3.576	3^-	3.578	3^-	48(1.5)	55(3)
3.598	5^-	3.594	5^-	3.600	5^-	12(0.8)	12(1.2)
		3.632	6^+				

Table 3 — continued

Ref. [9]		(p,p′), (d,d′) [a]		Present experiment			
E_x (MeV)	J^π	E_x (MeV)	J^π	E_x (MeV)	J^π	$\sigma(10°)$ (μb/sr)	σ_{max} (μb/sr)
3.670	$2^+, 3^+$						
		3.675	6^+				
3.705	(5^-)			3.704	5^-	69(2)	80(4)
3.710	$(3)^-$	3.707	(3^-)				
		3.762	(0^+)				
3.779	3^-	3.783	3^-				
		3.806	(4^+)				
		3.834	(0^+)				
3.870	$(4)^-$	3.871	$(4^-, 5^-)$				
				3.872	3^-	14(1)	14(0.7)
		3.897	$(0^+, 2^+)$	3.896	2^+	25(1.2)	44(4)
3.908	2^-	3.907	(5^-)				
				3.918	$2^+ + 5^-$	12(1)	20(4)+6(1.2)
		3.922	(1^-)				
		3.982	6^+	3.983	6^+	9.4(1)	16(0.8)
		4.003	4^+	4.004	(4^+)	18(1)	20(1)
4.010	$2^+, 3^+$						
				4.062	(5^-)	3.9(1)	4(0.6)
		4.102	4^+	4.096	4^+	5.3(1)	8(0.8)
4.1449	(1^-)						
		4.151	(5^-)	4.146	5^-	8(1)	11(1)
				4.169	2^+	17(1.2)	25(2)
		4.178	(4^+)				
				4.189	1^-	34(1.4)	78(11)
		4.199	2^+				
				4.260	4^+	18(1.1)	22(1.1)
		4.270	5^-				
		4.283	$(3^-, 4^+)$	4.286	4^+	15(1.1)	22(2.2)
		4.296	(5^-)				
		4.323	6^+				
		4.343	6^+				
4.382	(1^-)	4.380	1^-				
				4.403	(4^+)	6.5(1)	7(1)
4.417	(3^-)	4.423	(3^-)	4.423	(3^-)	10(1)	12(1.5)
		4.453	3^-				
		4.478	(4^+)				
				4.480	(5^-)	3(0.9)	3.5(0.5)
		4.494	2^+	4.497	(2^+)	6.8(1.2)	7(1)
		4.511	3^-				
		4.563	2^+	4.557	2^+	47(2)	85(13)
		4.577	2^+				
				4.615	2^+	111(3)	170(17)
		4.622	(3^-)				
		4.634	(2^+)				
		4.658	5^-				
		4.664	5^-				
				4.682	(6^+)	12(2)	10(1.5)

Table 3 — continued

Ref. [9]		(p,p′), (d,d′) [a]		Present experiment			
E_x (MeV)	J^π	E_x (MeV)	J^π	E_x (MeV)	J^π	$\sigma(10°)$ (μb/sr)	σ_{max} (μb/sr)
		4.702	3^-				
				4.712	$(1^-,2^+)$	21(2)	32(4)
				4.735	(3^-)	5.4(1.5)	7(1.4)
		4.739	(0^+)				
		4.747	6^+				
		4.793	3^-	4.793	(3^-)	14(2)	15(1.8)
				4.818	$(2^+,3^-)$	21(2)	24(3.6)
		4.833	(3^-)				
		4.842		4.837		10(2)	10(1)
		4.887	3^-	4.888	(4^+)	22(2)	30(3)

[a] Ref. [3].
[b] Corrected for two-step contributions.

(iii) since the level density becomes very high, different reactions can excite different levels lying within the uncertainty of the energy scale.

Since part of the states seen for the first time in the present experiment are weakly populated, one must take into account the possibility that some peaks observed in the energy spectra could be due to contaminants: other elements as well as other Nd isotopes. Considering the chemical purity of the targets and their isotopic enrichment, only the most intense transitions of each contaminant can give an observable yield. The target with the lowest enrichment was that used to study the ^{148}Nd(p,t) reaction. The peaks originated in the energy spectrum by the g.s. transition in the Nd contaminants are easily detected. The small peaks at 0.694, 0.945 and 1.316 MeV in the energy spectrum given in the lower part of Fig. 1 are due to g.s. transitions in ^{146,145,144}Nd(p,t)^{144,143,142}Nd, respectively. The few other transitions with a comparable yield, due to the same isotopes, can be easily discarded since their position and intensity is known from the present and other experiments. Spurious peaks from contaminants with masses different from those of Nd isotopes can be identified since their position moves with the reaction angle. By this kinematical effect it is possible to discard peaks produced by contaminants with a mass difference of the order of 10 mass units. Therefore only a very limited number of nuclei (some Ba, Ce, Sm and Gd isotopes) could give some effect. Their presence should, however, be evidenced by the respective g.s. transition. The identification of peaks from contaminants becomes difficult at high excitation energies, because of the high level density. Their overlap at certain angles can produce a distortion of the angular distribution in Nd transitions. This could explain the fact that some transitions at high excitations display an angular distribution, which cannot be reproduced by DWBA calculations.

Also due to the fact that weak transitions have been detected in these experiments, several states are seen both in the inelastic scattering and in the (p,t) experiments. For instance, 32 states with $J^\pi = 2^+$ have been detected in ^{146}Nd below 3.8 MeV. Of

Table 4
Same as in Tables 2 and 3 for ^{144}Nd

Ref. [10]		(p,p′), (d,d′) [a]		Present experiment			
E_x (MeV)	J^π	E_x (MeV)	J^π	E_x (MeV)	J^π	$\sigma(10°)$ (μb/sr)	σ_{max} (μb/sr)
0.000	0^+	0.000	0^+	0.000	0^+	639(5)	650(30)
0.6965	2^+	0.696	2^+	0.696	2^+	9.2(0.6)	80 [b](20)
1.3145	4^+	1.314	4^+	1.314	4^+	60(1.5)	60(6)
1.5105	3^-	1.510	3^-	1.510	3^-	23(1)	72 [b](14)
1.5619	2^+	1.561	2^+	1.561	2^+	37(1)	70(5)
1.7914	6^+	1.791	6^+	1.791	6^+	38(1)	40(4)
2.0727	(2^+)	2.073	2^+	2.073	2^+	33(1)	68(4)
2.0844	0^+			2.084	0^+	28(1)	30(2)
2.0934	5^-	2.093	5^-				
2.1094	(2^+)	2.109	4^+	2.109	$(1^-,2^+)$	5.9(0.5)	7(1)
2.1856	1^-	2.185	(1^-)	2.189	(1^-)	2.3(0.3)	4(0.6)
2.2181	(6^+)	2.217	6^+	2.220	6^+	2.9(0.3)	2.5(0.4)
2.2701	2^+						
2.2951	$(2,3,4)^+$	2.295	(4^+)	2.296	(4^+)	1.8(0.3)	1.7(0.3)
2.3217		2.327	(0^+)	2.328	0^+	4(0.4)	4(0.4)
2.3682	$(2)^+$	2.367	2^+	2.369	2^+	13.2(0.7)	26(1)
2.4472	2^+						
2.4512	4^+	2.451	4^+	2.451	4^+	42(1.2)	42(3)
2.5269	2^+	2.527	2^+	2.527	2^+	1.5(0.3)	6 [b](1.8)
2.5917	2^+	2.590	(1^-)				
2.6050	3^-	2.606	3^-	2.599	3^-	12(0.7)	16(0.8)
2.6125	(7^-)			2.613	$6^+(7^-)$	5.5(0.5)	10(0.5)
2.6546	3^+			2.656	(4^+)	19(0.8)	19(1)
2.6753	0^+	2.675	0^+	2.675	0^+	60(1.5)	60(3)
2.6926	(1,2)	2.694	2^+	2.693	2^+	9(0.6)	20(3)
		2.717	(1^-)				
2.7323				2.732	(3^-)	5.6(0.5)	8(0.8)
2.7789		2.779	3^-	2.779	3^-	7.7(0.6)	20 [b](6)
2.8391	(1,2)	2.833	3^-	2.837	$(2^+ + 3^-)$	6.7(0.5)	8(1.6)+6(1.2)
2.8675				2.868	(2^+)	4.3(0.5)	8.5(0.8)
				2.896		2.7(0.4)	2.2(0.3)
2.9004	$(2^+,3^+)$	2.898	2^+				
2.9677		2.969	3^-	2.969	(3^-)	10.3(0.7)	14(0.2)
2.9862		2.987	4^+	2.986	4^+	3.1(0.5)	3.2(0.4)
3.0262	(4^+)	3.026	5^-	3.027	4^+	56(1.4)	50(5)
3.0431	(3,4)						
		3.049	5^-	3.047	(5^-)	15(0.9)	15(2)
3.1008	(2,3,4)	3.097	$(0^+,2^+)$	3.098	2^+	31(1)	62(3)
3.1263	(2,3,4)			3.126	4^+	16(0.9)	15(2)
		3.130	1^-				
				3.157	0^+	88(2)	100(10)
		3.180	(6^+)				
		3.214	3^-				
3.2219				3.220	2^+	5.1(0.6)	12(1.8)
		3.240	(3^-)				

Table 4 — continued

Ref. [10]		(p,p′), (d,d′) [a]		Present experiment			
E_x (MeV)	J^π	E_x (MeV)	J^π	E_x (MeV)	J^π	$\sigma(10°)$ (μb/sr)	σ_{max} (μb/sr)
3.2925		3.289	(3^-)	3.290	3^-	48(1.4)	64(6)
3.3416		3.340	$(3^-,4^+)$	3.342	3^-	11(0.8)	15(3)
3.3817	$(\leqslant 4)$	3.382		3.382	2^+	96(2)	170(8)
		3.401	$(2^+,5^-)$	3.404	2^+	42(1)	90(4)
				3.432	5^-	7.5(0.7)	10(1.2)
3.4611		3.461	4^+	3.462	(4^+)	23(1)	20(1.5)
3.4942		3.493	5^-	3.490	5^-	13(2)	16(0.8)
		3.522	(2^+)				
				3.534	2^+	87(2)	150(7)
		3.555	(2^-)				
				3.589	3^-	25(1)	36(3)
3.6602		3.658	3^-	3.661	3^-	11(1)	17(2)
				3.678		8.7(0.8)	10(1.5)
				3.702	2^+	24(1)	44(2)
				3.731	2^+	9.3(0.9)	22(3)
				3.759	6^+	6.6(0.8)	8(1)
				3.796		4.1(0.8)	5(1)
				3.813	2^+	6.5(0.9)	17(2)
				3.834	(1^-)	11(1)	25(5)
				3.853	0^+	7.4(0.3)	8(1)
				3.871		3.1(0.8)	10(1.5)
				3.902	(1^-)	14.2(1)	30(7)
				3.933	$(6^+,7^-)$	4.1(0.9)	10(1.8)
				3.975	2^+	10(1)	26(5)
				4.032	(6^+)	2.4(1)	6(0.9)
				4.106	7^-	5.6(1)	10(1.8)
				4.133	(1^-)	23(1)	40(8)
				4.184	3^-	20(1)	27(2)
				4.227	(3^-)	20(1)	32(6)
				4.299	4^+	14(1)	15(1.5)
				4.317	2^+	16(1)	31(2)
				4.344	3^-	17(1.5)	21(2)
				4.415	5^-	14(1)	15(1.7)
				4.469	3^-	27(2)	34(3)
				4.543	(3^-)	51(2)	60(7)
				4.635	(2^+)	12.3(1.6)	25(3)
				4.657	(2^+)	21(1.7)	22(5)
				4.685	(7^-)	8(2)	7(1.4)
				4.845	(2^+)	26(2)	40(5)
				5.023	$(5^-,6^+)$	7.7(2)	10(1.5)

[a] Ref. [3].

[b] Corrected for two-step contributions. Other levels, for which the spin-parity has not been determined are located at 4.004 (5), 4.708 (5), 4.765 (22), 4.794 (34), 4.821 (32) and 4.885 (25)MeV. The cross section values at 10°, in μb/sr, are given in parenthesis.

Table 5
Same as in Tables 2 and 3 for ^{146}Nd

Ref. [11]		(p,p'), (d,d') [a]		Present experiment			
E_x (MeV)	J^π	E_x (MeV)	J^π	E_x (MeV)	J^π	$\sigma(10^\circ)$ (μb/sr)	σ_{max} (μb/sr)
0.000	0^+	0.000	0^+	0.000	0^+	827(12)	2200(110)
0.4538	2^-	0.454	2^+	0.454	2^+	98(4)	150 [b](8)
0.9155	0^+	0.918	0^+				
1.0431	4^+	1.043	4^+	1.042	4^+	30(2)	33(1.7)
1.1895	3^-	1.190	3^-	1.189	3^-	4.3(0.9)	50 [b](12)
1.3032	2^+			1.303	0^+	3.6(0.8)	10(1)
1.3767	1^-	1.376	1^-	1.377	(1^-)	1.2(0.5)	3(0.6)
1.4706	2^+	1.471	2^+	1.471	2^+	10(1)	10(1)
1.5177	5^-	1.517	5^-	1.517	5^-	1.6(0.5)	2.6(0.3)
		1.572	(0^+)				
1.6027	0^+			1.603	0^+	279(7)	550(50)
1.6971	0^+	1.695	(0^+)	1.697	0^+	16(2)	38(4)
1.7451	4^+	1.744	4^+	1.745	4^+	45(3)	53(5)
1.7772	3^+			1.777	$(3^+,4^+)$	1(.4)	1.3(0.3)
1.7801	6^+	1.780	6^+				
1.7874	2^+	1.787	2^+	1.787	2^+	25(2)	30(1.5)
1.9054	2^+			1.905	2^+	3(0.7)	5(0.5)
1.9184	4^+	1.917	(4^+)				
1.9779	2^+	1.976	(2^+)	1.978	2^+	50(3)	61(3)
1.9893	4^+	1.988	4^+	1.990	(4^+)	1.5(0.5)	3.3(0.5)
2.0295	7^-	2.027	1^-				
2.0458	5^-						
2.0726	4^-	2.069	5^-				
				2.084	(6^+)	21(2)	30(3)
		2.090	(0^+)				
2.0961	(4^+)			2.095	(4^+)	2.5(0.7)	3.4(0.7)
2.1439	$(1^+,2^-)$			2.142	(2^+)	1.6(0.5)	1.8(0.3)
2.1673	3^-			2.171	(3^-)	0.3(0.2)	0.9(0.2)
2.1974	2^+	2.198	2^+	2.197	(2^+)	1.2((0.5)	2.3(0.5)
2.2084	2^+						
2.2258	$(3,4)^+$	2.225	1^-				
2.2323	3^-			2.227	3^-	2.9(0.7)	4.6(0.7)
2.2659	2^+	2.269	1^-	2.267		4.3(0.9)	5.8(0.8)
2.2864	2^+			2.286	0^+	49(3)	160(16)
2.3357	3	2.335	3^-	2.335	(3^-)	4.4(0.9)	11(1)
2.3565	2^+			2.357	(4^+)	33(2)	31(4)
2.4349	4^+						
2.4366	$(2,3)^+$			2.438	2^+	6.3(1)	7(0.7)
2.4572	2^+	2.453	2^+				
2.4749	8^+	2.478	(2^+)	2.474	$2^+ + (7^-,8^+)$	4.2(1)	4(0.8)+1.4(0.5)
2.5209		2.525	3^-	2.522	$(4^+,5^-)$	9.2(1.3)	14(1.4)
2.5288				2.529	2^+	2.2(0.6)	3.4(0.7)
2.5528	2^+	2.552	4^+	2.552	(2^+)	2(0.9)	2(0.3)
		2.570	5^-				
2.5743				2.574	2^+	58(3)	79(4)
2.5908				2.587	2^+	2.1(0.6)	3.8(0.4)

Table 5 — continued

Ref. [11]		(p,p'), (d,d')[a]		Present experiment			
E_x (MeV)	J^π	E_x (MeV)	J^π	E_x (MeV)	J^π	$\sigma(10°)$ (μb/sr)	σ_{max} (μb/sr)
2.616				2.612	0^+	50(3)	92(9)
		2.622	4^+	2.623	4^+	2(0.6)	3(0.4)
				2.641	(1^-)	2.8(0.7)	6(1)
2.6608		2.665	2^+	2.663	(1^-)	34(3)	40(6)
		2.687	(3^-)	2.690		3.1(0.7)	6(0.6)
2.7057	(2^-)						
		2.705		2.706	(4^+)	7(1)	10(0.5)
				2.729	0^+	143(5)	250(25)
2.7501		2.747	5^-	2.749	5^-	3.1(0.7)	4.4(0.4)
2.8040		2.807	(4^-)	2.806		8(1)	8(1)
		2.821	3^-	2.820	0^+	100(4)	176(17)
2.8446		2.847	3^-	2.845	(3^-)	8(1)	8(1)
				2.856	3^-	4.3(0.9)	5.6(0.5)
2.8706		2.874	(2^+)	2.871	2^+	63(3)	72(3)
2.8853		2.887	(4^+)	2.885	(4^+)	24(2)	24(3)
2.9136		2.916	4^+	2.917		3(0.7)	4.8(0.7)
2.9291		2.932	3^-	2.930	3^-	10(1)	13(0.6)
		2.945	(0^+)	2.945	0^+	74(4)	138(11)
2.9696		2.973	2^+	2.970	2^+	11(1)	16(1.6)
2.9967				2.993	3^-	12(1)	15(0.7)
3.0042		3.005	5^-				
3.0133		3.017	3^-				
3.028				3.028	0^+	30(2)	66(5)
3.0347		3.038		3.039	(2^+)	37(3)	58(6)
3.0423				3.047	2^+	18(2)	34(5)
3.0912		3.094	4^+	3.093	2^+	11(1.4)	11(1)
		3.102	2^+				
		3.129	(1^-)	3.126	1^-	27(2)	50(5)
		3.149	6^+	3.148	4^+	5(1)	9(1.3)
		3.161	4^+				
				3.178	2^+	22(2)	30(1.5)
		3.208	4^+				
				3.220	2^+	23(2)	30(1.5)
		3.230	(4^-)				
				3.236	2^+	22(2)	26(1.3)
		3.248	3^-				
3.272		3.272	(6^+)				
		3.284	2^+	3.283	2^+	21(2)	26(1.3)
		3.310	4^+				
3.3289				3.329	2^+	40(3)	56(3)
3.355		3.354	3^-	3.356	(3^-)	27(2)	32(1.6)
3.3690				3.368	3^-	19(2)	30(2.4)
3.391				3.389	1^-	11(1.4)	38(6)
		3.420	(0^+)	3.419	0^+	33(2)	70(7)
		3.434	5^-				
				3.443	2^+	15(1)	18(1)

Table 5 — continued

Ref. [11]		(p,p′), (d,d′) [a]		Present experiment			
E_x (MeV)	J^π	E_x (MeV)	J^π	E_x (MeV)	J^π	$\sigma(10°)$ (μb/sr)	σ_{max} (μb/sr)
3.453		3.453	4^+	3.455	4^+	5.2(1)	10(1)
		3.471	$(3^-,4^+)$	3.468	3^-	30(2)	38(2)
		3.484	2^+	3.481	2^+	7(1)	7(0.7)
		3.499	5^-	3.496	$(5^-,6^+)$	6.6(1.2)	7(0.7)
				3.521	3^-	3.6(2)	4(0.2)
				3.531	1^-	30(2)	52(0.8)
		3.537	2^+	3.546	(2^+)	9(1)	9(1)
		3.563	5^-	3.558	(5^-)	12(1.6)	17(1.7)
				3.569	2^+	18(2)	22(1.1)
		3.583	2^+				
3.5947				3.601	4^+	14(1.6)	14(2)
		3.614	5^-	3.610		14(1.6)	20(4)
		3.622	2^+	3.625	(2^+)	7.2(1.2)	9(0.5)
				3.646		9.4(1.4)	14(2)
		3.672	5^-	3.667	5^-	47(3)	50(4)
3.668				3.670	(2^+)	45(2)	90(4)
				3.692	(5^-)	8(1.4)	7(1.4)
				3.701	(2^+)	5(19	6(1.2)
3.7092				3.712	2^+	15(2)	15(1.5)
				3.727	2^+	7(1.2)	12(0.6)
				3.742	3^-	28(1.2)	36(2)
		3.753	(4^+)	3.754	1^-	25(2)	50(3)
				3.762		3(1)	9(2)
				3.782	(2^+)	4.8(1)	4(0.8)
				3.789		1(0.4)	3(0.6)
				3.810	3^-	29(2)	34(3.4)
				3.830		6(1.2)	5(0.8)
				3.847		2(0.6)	3(0.6)
				3.866	(2^+)	6(1)	11(1)
				3.875	(5^-)	6(1)	5(0.7)
				3.884	(4^+)	6(1)	6(0.9)
				3.892		1.4(0.6)	2.8(0.3)
				3.913	(3^-)	7.6(1.2)	12(1.8)
				3.922	3^-	4(1.4)	7(0.7)
				3.931		6(2)	7(1)
				3.939	(2^+)	9.2(1.4)	24(2.4)
				3.949	(2^+)	7(1.2)	7(1)
				4.006	(2^+)	4.6(1)	14(2)
				4.039	$(2^+,3^-)$	10(1.6)	10(1.4)
				4.054	(2^+)	14(1.6)	15(1.5)
				4.066	(2^+)	4.2(0.8)	13(2)
				4.121	(2^+)	14(2)	22(2.2)
				4.138	$(2^+,3^-)$	14(1.6)	17(1.7)
				4.168	2^+	15(1.6)	36(3.6)
				4.179	3^-	12(1.6)	20(2)
				4.196	2^+	10(1.4)	12(0.6)
				4.212	2^+	9(1.4)	24(2.4)
				4.243	1^-	36(2)	60(9)

Table 5 — continued

Ref. [11]		(p,p′), (d,d′) [a]		Present experiment			
E_x (MeV)	J^π	E_x (MeV)	J^π	E_x (MeV)	J^π	$\sigma(10°)$ (μb/sr)	σ_{max} (μb/sr)
				4.256	2^+	9.6(1.4)	28(2)
				4.302	(4^+)	7(1.2)	7(0.7)
				4.310	(1^-)	8.4(1.2)	10(2)
				4.325	(4^+)	7.6(1.2)	7.6(1.5)
				4.341	$(2^+,3^-)$	6.4(1.2)	15(1.5)
				4.380	(3^-)	7.6(1.2)	18(1.8)
				4.388	(2^+)	8.6(1.2)	20(2)
				4.404	4^+	5(1)	7(1)
				4.411	(4^+)	5.2(1)	6(0.9)
				4.422	(3^-)	7(1.2)	9(1.4)
				4.442	3^-	8.2(1.2)	14(1.4)
				4.461	(3^-)	9(1.4)	18(2.1)
				4.491	(3^-)	9(1.4)	9(0.8)
				4.501	(3^-)	7(1.2)	16(3)
				4.517	(4^+)	13(1.6)	13(1.8)
				4.533	(3^-)	9(1.4)	16(3)
				4.545	4^+	8(1.4)	8(0.8)
				4.558	(3^-)	7.4(1.2)	15(2)
				4.571	(3^-)	11(1.2)	13(2)
				4.591	$(2^+,3^-)$	9.6(1.4)	13(2)
				4.649	(3^-)	9.6(1.4)	17(2.5)
				4.696	(3^-)	9(1.6)	18(2.4)
				4.707	(3^-)	8(1.2)	10(1.5)
				4.738	3^-	12(1.6)	24(2.4)
				4.755	3^-	12(1.6)	13(2)
				4.765	2^+	7(1.2)	10(1)
				4.802	(3^-)	10(1.4)	16(3)
				4.899	4^+	7.6(1.2)	9(1.3)
				4.948	(4^+)	1.2(1.6)	10(1)
				4.964	(3^-)	10(1.4)	13(2.6)
				4.982	3^-	11(0.4)	14(1.2)

[a] Ref. [3].

[b] Corrected for two-step contributions. Other levels for which the spin-parity has not been determined are located at 4.022 (2), 4.031 (6), 4.095 (13), 4.269 (17), 4.360 (7), 4.479 (21), 4.601 (9), 4.637 (9), 4.669 (21), 4.683 (10), 4.720 (20), 4.773 (14), 4.784 (12), 4.794 (7), 4.822 (16), 4.832 (15), 4.860 (6), 4.866 (10), 4.877 (7), 4.887 (12), 4.911 (13), 4.931 (12). The cross section values at 10°, in μb/sr, are given in parenthesis.

these 12 are seen both in (p,p′) and (p,t) reactions, 3 only in (p,p′) and 21 only in (p,t). This is evidence that a part of the collective p–h configurations is mixed with h–h configurations. Also for the other multipolarities in ^{146}Nd as well as in ^{144}Nd the fraction of states which have been detected in both reactions is at least 1/3. In ^{142}Nd this fraction is only 1/4. The summed cross section, at the maximum of the angular distributions, for the excitation of 2^+ states in ^{142,144,146}Nd by the (p,t) reaction is of the order of 1–2 mb/sr. The transitions to states detected also in inelastic scattering account for the 43% of this cross section in ^{144,146}Nd and the 22% in ^{142}Nd. Also for

Table 6
Optical-model parameters used in DWBA and CC calculations. The well depths are in MeV and the geometrical parameters in fm

Particle	V_0	r_0	a	W	W_D	r_w	a_w	V_{s0}	r_{s0}	a_{s0}	r_c
Neutrons	[a]	1.25	0.65					6.2			
Protons	[b]	1.17	0.71	2.13	[c]	1.27	0.65	6.2	1.01	0.75	1.20
Tritons	175.	1.142	0.75	17.4		1.60	0.86				1.25

[a] Adjusted by reproducing the two-neutron separation energy.
[b] 54.6 and 57.6 MeV at 35.6 and 25 MeV incident energy, respectively.
[c] 8.05 and 7.80 MeV at 35.6 and 25 MeV incident energy, respectively.

the 4^+ states the lowest percentage is found in ^{142}Nd. This indicates a larger decoupling in this last nucleus of the collective states from h–h states, certainly due to the closure of the neutron shell at $N = 82$. A different trend is found for the above percentage in the case of the transitions to the 3^- states: 72, 80 and 62% for ^{142}Nd, ^{144}Nd and ^{146}Nd, respectively. The different trend for 3^- states could be due to the fact that these transitions involve rearrangements between major shells. Finally it should be remarked that the ^{142}Nd(p,t) reaction displays cross sections larger than those for the other targets.

3. DWBA and coupled-channels calculations

The spin-parity assignments of Tables 2–5 have been obtained from the comparison between experimental and calculated differential cross sections. The DWBA calculations were performed using the computer code DWUCK4 [13], with the optical-model parameters given in Table 6. These parameters belong to standard families and have been adjusted slightly to give a better agreement with the shape of the experimental angular distributions. Those for protons were derived from Becchetti–Greenlees optical model potentials [14], while those for tritons belong to a family often used (Bes et al. [2]) in the analysis of nucleon transfer reactions: $V_0 = 160$–170 MeV, $W \geqslant 16$ MeV, $W_D = 0$ and $r_w \gg r_0$.

Microscopic transition form factors produced by the code have been used. These form factors were obtained by coupling two neutrons in model states with binding energies in agreement with the experimental separation energies. A total of 28 neutron shells with $j \leqslant \frac{19}{2}$ were included in the calculations. The number of different neutron pairs and relative form factors, obtained coupling two neutron configurations is 28 for $L = 0$ and always larger than 100 for other L-transfers. For a given L-transfer, the different form factors give differential cross sections with an absolute value that is changing strongly with the configurations considered, but with very similar angular distributions. The choice of the form factor does not affect, therefore, the spin-parity assignment.

Most transitions show an angular distribution characteristic of a given L-transfer, which leads to an unambiguous assignment of J^π to the final state. Examples of fits of good quality obtained by DWBA calculations are given in Fig. 2. The dependence

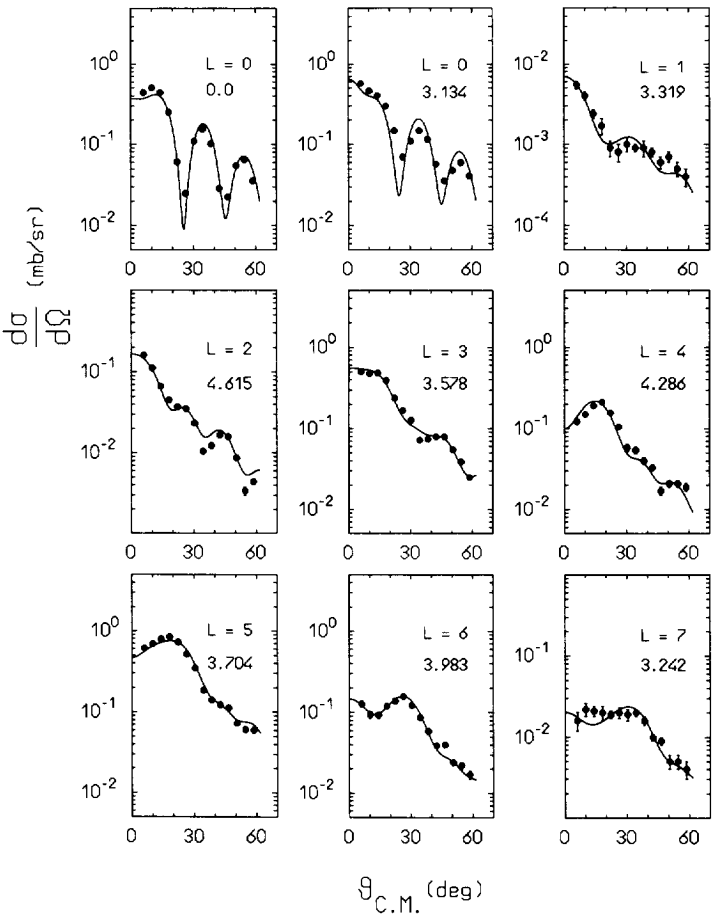

Fig. 2. Differential cross sections for different L-transfers observed in the ^{144}Nd(p,t)^{142}Nd reaction. The full curves are from DWBA calculations. The excitation energies (in MeV) and the transferred angular momenta are indicated in the figure.

of the angular distributions on the transferred angular momentum is clearly shown. The quality of the experiment and of the analysis can be assessed from a larger sample of data. The differential cross sections of the transitions leading to the 2^+ states in ^{144}Nd, are given in Fig. 3. The $L = 3$ transitions to the 9 higher-lying 3^- states of the same nucleus and the full set of $L = 4$ transitions are given in Fig. 4. It is worthwhile to point out that, in spite of the fact that the ^{146}Nd(p,t) reaction has been measured with the worst ratio between level density and resolving power and that several transitions are very weak, the agreement between data and DWBA calculations is rather satisfactory.

The DWBA analysis gave information on the spin-parity of about 300 states out of the 350 peaks observed in the energy spectra. Some peaks display an angular distribution that does not correspond to any pure L-transfer and consequently the angular momentum transferred is not easily determined. At high excitation energies this could be due

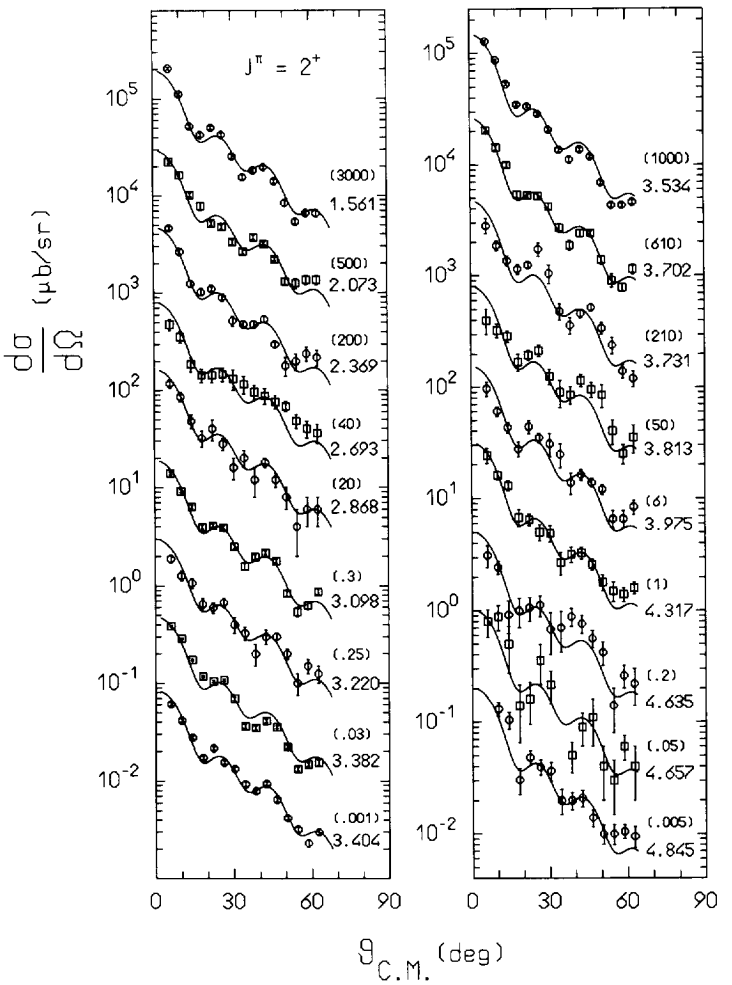

Fig. 3. Differential cross sections for the excitation of 2^+ states by the ^{146}Nd(p,t)^{144}Nd reaction. The full curves are from DWBA calculations. The numbers in round brackets are the multiplication factors used in plotting the data.

to the overlap with other levels or contaminants at some angles. However, the J^π assignments are mostly in agreement with the previous ones. The most interesting cases of assignments in contrast with previous studies are shown in Fig. 5: the full and dashed curves have been obtained using the present and the previous J^π assignment, respectively. In principle different reactions can excite different states lying at an approximately equal excitation energy. However, this explanation is less probable in the case of states lying below or near 2 MeV excitation energy, where the uncertainty in the energy scale is very small ($\leqslant 2$ keV) and the level density is relatively low.

In Nd(p,t) reactions the best matching conditions in angular momenta are at 35.6 MeV for a momentum transfer of $L = 4$ and at 25 MeV for $L = 3$–4. This means that final

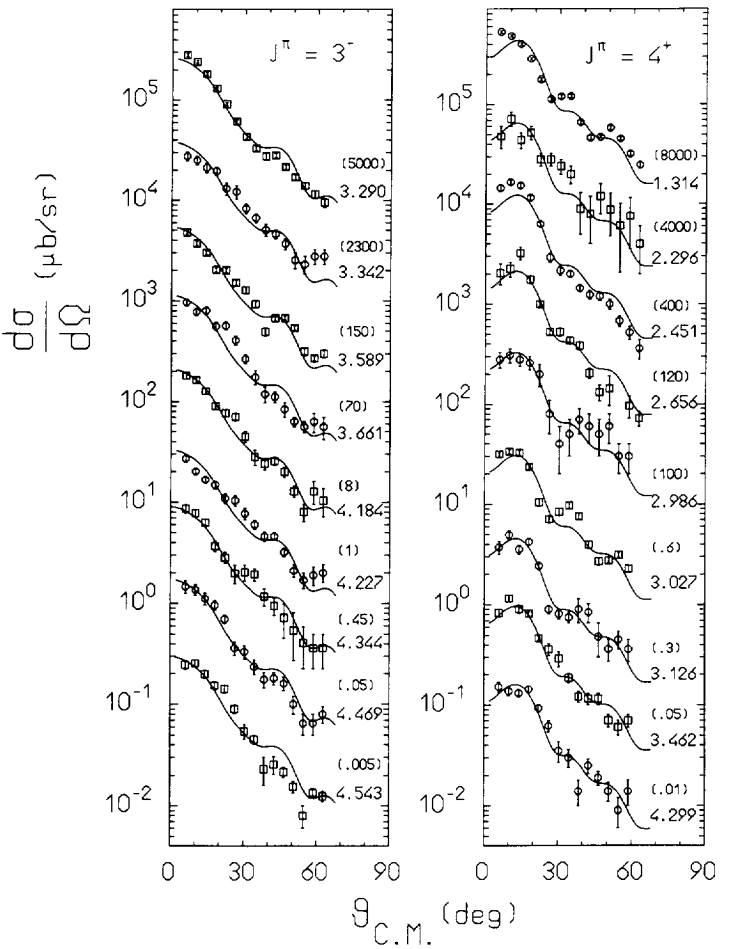

Fig. 4. Same as in Fig. 3 for the excitation of the 3^- states (left side) and the 4^+ states (right side).

states with a spin up to $J = 6$–7 are reasonably well excited. In fact several final states with $J^\pi = 6^+$ and 7^- have been detected. The differential cross sections for the excitation of a part of these states, not seen in previous studies, are shown in Fig. 6.

As was already observed [7], the DWBA fails to account for the measured angular distribution of certain transitions. This is the case of the transitions leading to the 2_1^+ and 3_1^- states. The excitation of these states receives large contributions from two-step processes: an inelastic excitation of the 2_1^+ (3_1^-) state in the target nucleus followed by a two-neutron transfer or, vice versa, a two-neutron transfer to the g.s. in the final nucleus followed by an inelastic excitation of the residual nucleus. One can estimate in a model independent calculation the cross section produced by the process $^{A}\mathrm{Nd(p,t)}^{A-2}\mathrm{Nd}_{gs}\mathrm{(t,t')}^{A-2}\mathrm{Nd}_{2_1}$, since the amplitudes of the first and second steps can be obtained directly from experiments. The cross section of this process alone is of the same order or larger than the experimental one, which on the other hand can receive important

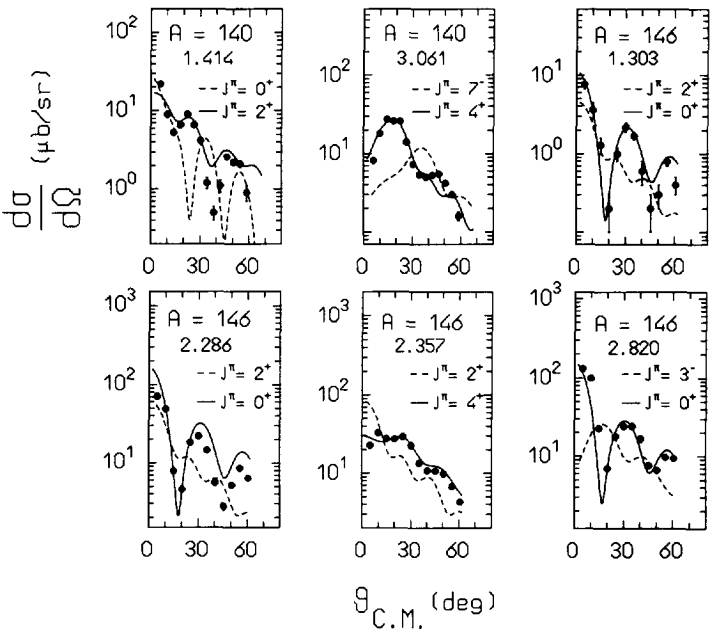

Fig. 5. Spin-parity assignments in contrast with previous studies. The mass and the excitation energy of the final nucleus are given in the figures. The full and dashed curves have been obtained with the present and the previous J^{π} assignment respectively.

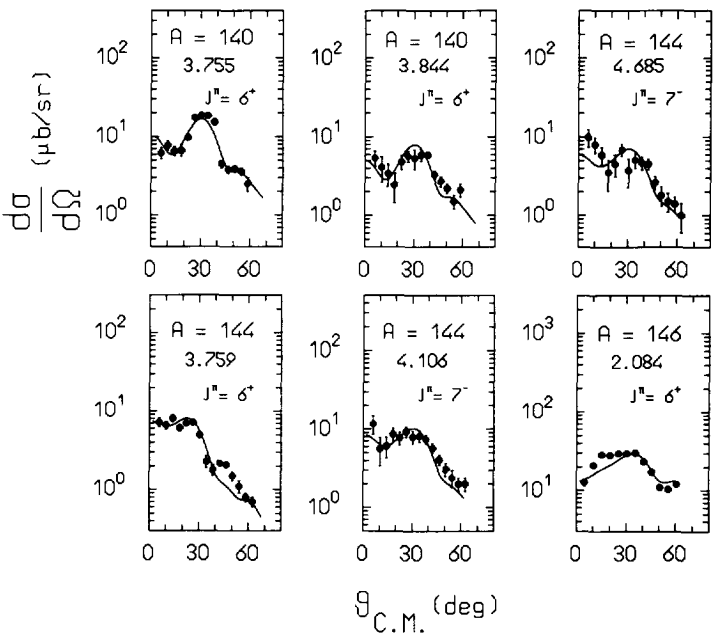

Fig. 6. Differential cross sections for the excitation of 6^{+} and 7^{-} states not seen in previous studies.

contributions also from another strong two-step process: $^{A}\mathrm{Nd}(\mathrm{p,p'})^{A}\mathrm{Nd}_{2_1^+}(\mathrm{p,t})^{A-2}\mathrm{Nd}_{2_1^+}$. For these transitions the experimental cross sections have been compared with coupled-channel (CC) calculations. The computer code CHUCK [13] has been used.

In previous studies [7,15] CC calculations have been performed using two-neutron configurations and their spectroscopic amplitudes from a nuclear structure model and the coupling amplitudes for the inelastic channels from models or from other experiments. Since the present study is aimed at deriving information on the residual interactions from the experimental $B(\mathrm{E}\lambda)$ and $\sigma(\mathrm{p,t})$ values, we followed a different procedure. The analysis of the transition to the 2_1^+ state, which is relevant in the present study, is here described. To reproduce this transition six sets of coupling parameters are needed: two for the inelastic channels and four for two-neutron transfer transitions. The β_2 deformation parameters in the target and the residual nucleus, which are known from inelastic scattering experiments, give the inelastic-scattering couplings. It can be noticed that the magnitude of these two parameters, i.e. the collectivity of target and residual nucleus, determines the relative importance of the two-step contributions. The two-neutron transfer amplitude for the transition $0_i^+ \rightarrow 0_f^+$ is easily fixed to reproduce the observed $\sigma(\mathrm{p,t})$ for the same transition. The other three couplings describe the transitions: $0_i^+ \rightarrow 2_f^+$, $2_i^+ \rightarrow 2_f^+$ and $2_i^+ \rightarrow 0_f^+$. These are obtained from a best fit of the data, using model predictions only as a starting point. Their values are affected by large errors, due to the ambiguities between the different parameters in search. The error in the value of the "direct" part of the cross section, due to the transition amplitude $0_i^+ \rightarrow 2_f^+$, can be of the order of 20–40%. In the case of the transition to the 2_1^+ state in ^{142}Nd the present analysis is in good agreement with that described by Yagi et al. in Ref. [7]. In spite of their large uncertainty these semiempirical cross sections are still significant for the comparison described in Section 6. In Fig. 7, two typical examples of CC calculations for the transitions to the 2_1^+ and 3_1^- states in ^{144}Nd are given. Similar CC calculations have been performed also for the other 2^+ and 3^- transitions for which the above two-step process is evidenced by similar angular distributions.

At low incident energies the (p,t) reaction can proceed by another two-step process: the sequential transfer of two neutrons. The analysis of the (p,t) reaction in terms of the p–d–t process is more difficult than that for a two-step process via the inelastic channels for several reasons:

(i) the number of the intermediate states and therefore of the possible channels is higher;

(ii) the singlet S-state and the D-state in the deuteron wave function open further reaction channels;

(iii) the coupling parameters for the first step can be easily derived or tested on (p,d) experiments, but not those that, in the second step, connect excited states in the intermediate and final nucleus.

A practical way, used by Igarashi et al. in a recent study [16], is to consider simple configurations with "realistic" spectroscopic amplitudes, it is to say of the order of those obtained from one-neutron pick-up data. They have shown, in the case of natural parity transitions, that the simultaneous and the sequential pick-up of two neutrons give

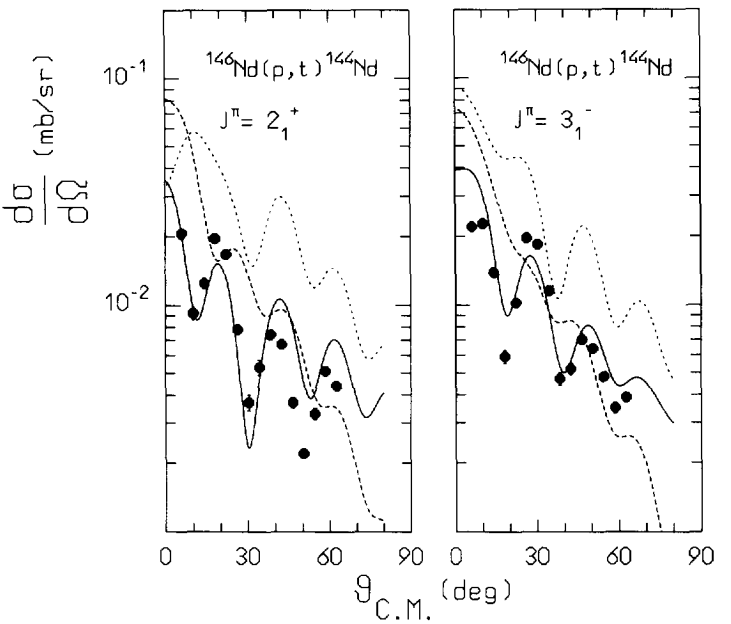

Fig. 7. Differential cross sections for the excitation of the 2_1^+ and 3_1^- states in ^{144}Nd. The full curves are from CC calculations (see text). The dashed curve is the cross section due to the direct transition only and the dotted curve shows the contribution of two step-processes. A destructive interference between the direct ant the two-step process is evident.

differential cross sections with similar angular distributions. This similarity makes it more difficult to distinguish among the different reaction mechanisms, but at the same time makes the spin-parity assignments more reliable. They have also shown that the sequential transfer mechanism can affect the absolute value of the cross sections, but does not invalidate the customary statement that the (p,t) reactions are good for probing nuclear correlations, since the two-step amplitude is also enhanced in the same way as the one-step process by the pair correlations.

Different is the case of the excitation of unnatural parity states. These states in fact cannot be excited by the one-step process and therefore they constitute a test of the importance of sequential transfers. The cross sections calculated as suggested above result of the order of 1 μb/sr. Cross sections of this order have been obtained in Ref. [16] in the case of the 3^+ states in ^{208}Pb at 35 MeV proton incident energies. Few unnatural parity states are known in the Nd isotopes. A 4^- state should be located at 2.9597 MeV in ^{142}Nd. This state cannot be identified with the 2.958 MeV level excited by a strong (p,t) $L = 0$ transition (see Fig. 8). Other unnatural parity states (a 4^- at 3.870 MeV in ^{142}Nd, a 3^+ state at 2.6546 MeV in ^{144}Nd and a 2^- state at 2.7057 MeV in ^{146}Nd) are located at excitation energies very near to levels that are excited by the (p,t) reaction with a cross section of the order of 10–20 μb/sr. These cross sections are larger than predicted for unnatural parity transitions: the dashed curves given in Fig. 8 have been obtained normalizing CC predictions by factors of the order of 10.

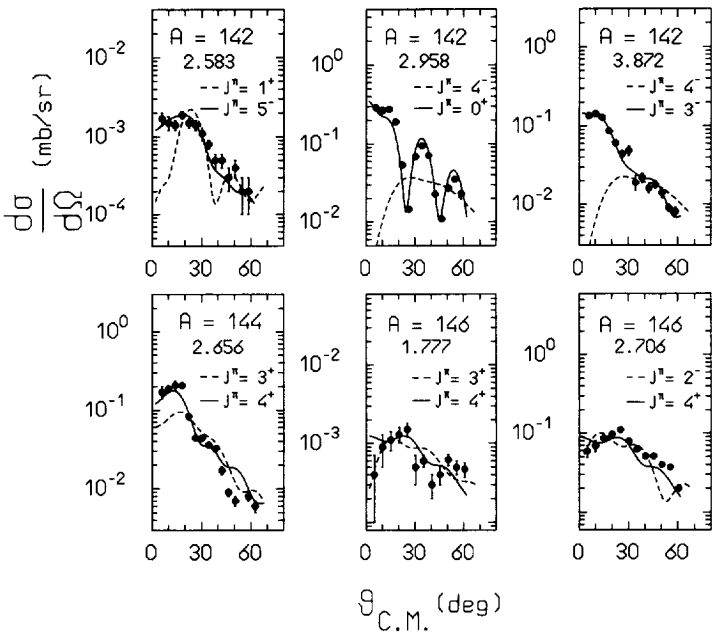

Fig. 8. Transitions to possible unnatural parity states. The dashed curves have been obtained from coupled channel calculations assuming a (p–d–t) reaction mechanism and the unnatural parity J^{π} assignment given in the figures. The full curves are from DWBA calculations assuming the direct excitation of a natural parity state.

Moreover, the experimental angular distributions are better reproduced as a direct two-neutron transfer with $L = 3$, 4 and 4, respectively. Two other states, a 3^+ at 2.5478 MeV and a 2^- at 3.807 MeV in ^{142}Nd were not seen in the present experiment. Finally two levels, located at 2.583 MeV in ^{142}Nd and at 1.777 MeV in ^{146}Nd, are excited in the (p,t) reaction with a cross section of 1.5–2 μb/sr. The absolute value of these cross sections is reproduced, within a factor of 2, as a sequential two-neutron pick-up to 1^+ and 3^+ states, respectively. Also the angular distributions are reasonably reproduced. In summary, both CC calculations and the experimental data indicate that the cross sections for the excitation of unnatural parity states should be of the order of 1 μb/sr.

Large uncertainties are found in the overall normalization of the calculated cross sections. These uncertainties must be considered in deriving information on g.s. correlations and residual forces. It is known [2,16] that zero-range DWBA calculations reproduce the angular distributions and the relative magnitude of (p,t) cross sections, but fail to reproduce their absolute values. The empirical value of the normalization constant, $D_0^2 N_t$, of zero-range DWBA calculations, is larger than D_0^2 by 1–2 orders of magnitude if the constant D_0 is obtained by simple theoretical considerations. Finite-range calculations improve the calculated absolute cross sections, but this is not sufficient to bridge the difference between theory and experiment. An N_t value, different from unity, could be due, in addition to the zero-range assumption, also to other effects coming for instance from the choice of the optical-model parameters, from the triton internal wave function

or from the sequential two-neutron transfers described above. We have used DWUCK and CHUCK codes and the zero-range approximation. In this case the empirical normalization factor N_t, as found in previous studies, is expected to have a value between 15 and 40 [2,16].

4. The 0^+ states and pairing vibrations

Several nuclear properties demonstrate the existence of pairing correlations in nuclei:
(i) the odd–even mass difference,
(ii) the energy gap in the low energy spectra of even nuclei,
(iii) the small value of the moment of inertia in deformed nuclei.
All these concern static properties of the pairing interaction. Other phenomena must be studied to have evidence on the dynamic aspects.

As mentioned above, the (p,t) reaction makes it possible to explore the dynamical effects of the pairing field. A large part of the previous (p,t) and (t,p) studies, both theoretical and experimental ones, were devoted to the analysis of $L = 0$ transitions. This is also because the energy spectra obtained from the two-neutron transfer reactions are dominated by these transitions. It has been shown that some features of the $L = 0$ transitions can be understood in terms of pairing vibrations and pairing rotations [2,17].

The pairing interaction can build strong correlations, which affect the single-particle motion by correlating a particle moving in a state with the particle moving in the time reversed state. This correlation changes the density distribution of particles around a given particle and produces a distortion of the Fermi surface, hereafter referred to as pairing distortion. For large values of the pairing field the nucleus reaches a superfluid state, the distinction between particles and holes is washed out and a given configuration has no more a definite number of particles. This is analogous to the quadrupole-deformed scheme, produced by the p–h interaction, where angular momentum is not conserved for particles moving in a deformed potential.

The addition (or removal) of two particles without changing the intrinsic state (no quasi-particle excitations) is the collective transition associated with the pairing distortion. Large cross sections are expected for the transfer of two identical nucleons among states in the same superfluid band. These transitions are the counterpart of E2 transitions among members of the same rotational band. Moreover, the fluctuations of the pairing field around its equilibrium value must be considered. These fluctuations give rise to collective oscillations, namely pairing vibrations, which are the analogues of nuclear shape vibrations in spherical or quadrupole-deformed states. This picture divides the $L = 0$ two-neutron transfer transitions in two distinct categories. Those connecting members of a pairing rotational band (for example g.s. to g.s. transitions) and those connecting states belonging to different bands. According to the estimates described in Ref. [2] one expects the spectrum to be dominated by the g.s. to g.s. transition. This picture agrees with experimental observations. Among the weaker transitions, the one corresponding to the pairing vibration (p.v.) is predicted stronger than others. The first

0^+ p.v. state, which is the counterpart of the two-phonon triplet in vibrational nuclei, is obtained from the g.s. of the residual nucleus by removing and adding pairs of neutrons, i.e. increasing by 1 the number of both p–p and h–h correlated pairs.

In closed-shell nuclei, the pairing correlations are not strong enough to overcome the single-particle energy gap and a permanent pairing distortion is not produced. These nuclei are called normal (in contrast to superfluid ones). Therefore a phase transition from normal to superfluid nuclei should occur, namely the change from the pairing-vibrational scheme into the pairing-rotational scheme, along a family of isotopes.

To compare the Nd data with the predictions of this schematic picture, we should recall here the most conspicuous features one expects to observe near a closed shell N_0:

(i) two-neutrons pick-up from the targets $N_0 + 2$, $N_0 + 4$, $N_0 + 6$, etc. will have an enhanced g.s. transition strength, varying like 1:2:3, etc.;

(ii) in each nucleus a strong transition to an excited 0^+ state should occur with a cross section and a Q value equal to that of the $|N_0\rangle \rightarrow |N_0 - 2, \text{g.s.}\rangle$ transition;

(iii) the g.s. energies should have a linear dependence with the number of pairs, namely $(E_{A+4} - E_A)/(E_{A+2} - E_A) = 2$.

For pairing rotations one expects:

(i) an enhanced and constant strength for the transitions listed in point (i) above.

(ii) a vanishing transition strength to the p.v. 0^+ state.

(iii) a quadratic trend of g.s. energies, namely $(E_{A+4} - E_A)/(E_{A+2} - E_A) = 4$.

Along the Nd family the g.s. energies, referred to the g.s. of ^{142}Nd, are: 2.00, 4.62, 7.93 and 11.45 MeV for A = 144, 146, 148 and 150, respectively. This trend is sligthly steeper than a linear dependence. Trache et al. [17], in the analysis of ^{145}Nd(p,t)^{143}Nd data, discussed the g.s. energies of the Nd isotopes in terms of the grand potential: total energy of the system minus the chemical potential times the number of pairs. They were able to reproduce the experimental trend assuming a vibrational scheme with anharmonic corrections.

The strengths of the L = 0 transitions studied in the present experiment are given in Fig. 9. The experimental cross sections are divided by σ_{DWBA} to facilitate the comparison between the different transitions. The values of σ_{DWBA} have been normalized to reproduce the experimental cross section for the transition ^{144}Nd(p,t)^{142}Nd$_{\text{gs}}$. The calculated cross section should take into account the different kinematical conditions for the different transitions. Namely the data are corrected for the dependence of the cross section on the incident energy, on the Q-value of the reaction and on the separation energy of the transferred pair of neutrons. The data given in the figure are therefore quantities proportional to the square of the spectroscopic amplitudes and are taken as (p,t) strengths in this analysis. The g.s. transition is always dominant, but several other 0^- states have been detected with a sizeable strength. The centroid of the strength of these excited 0^+ states is located at 2.7–2.9 MeV. Some of these strengths are given in Table 7 together with the predictions for pairing vibrations and rotations. For the strength of the transition to the p.v. state in each nucleus one can assume that of the strongest transition to an excited 0^+ state or the summed strength of the transitions located around the excitation energy predicted (see the point (ii) above) for the p.v.

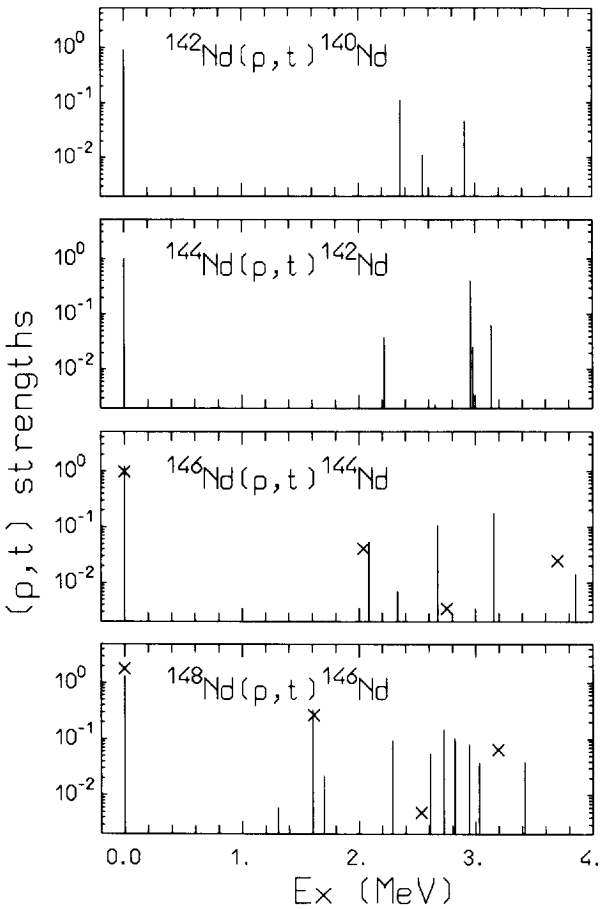

Fig. 9. Experimental transition strengths (square of transition amplitudes deduced from DWBA calculations) for the excitation of 0^+ states. The strengths are normalized to the amplitude for the ground-state transition in the ^{144}Nd(p,t)^{142}Nd reaction (see text). The crosses in the two lowest figures are from IBM calculations.

state (in our case 2.5–3.0 MeV). The first prescription leads to identify the states at 2.958, 3.157 and 1.603 MeV in ^{142}Nd, ^{144}Nd and ^{146}Nd respectively, as p.v. states. With the second prescription, summing up the strength between 2 and 3.2 MeV, the p.v. state should have a centroid at 2.88, 2.84 and 2.74 MeV in ^{142}Nd, ^{144}Nd and ^{146}Nd, respectively. The strengths for the excitation of the p.v. states are given in the last column of Table 7. The first and the second number written in parenthesis are the strengths obtained using the first and second prescriptions, respectively. As for the g.s. energies the experimental trend of the cross sections is intermediate between that of a pairing vibrator and that of a pairing rotator. From the analysis of 0^+ data, one can therefore conclude that the Nd isotopes constitute a transitional region.

A different approach to study transitional nuclei can be found in the framework of the Interacting Boson Model (IBM). The U(5) and SU(3) limits correspond to the pairing vibrations and rotations respectively. The IBM model includes also the O(6)

Table 7
Strengths of (p,t) transitions leading to the 0^+ ground state and to the 0^+ pairing vibrational states in the final nucleus. The values given in the table have been normalized to the strength of the transition to $^{142}Nd_{gs}$. The predictions of the schematic model of Ref. [2] are given in columns 2 and 3. The experimental strengths are given in column 4. The numbers in parenthesis are the strengths summed over the 0^+ levels lying at excitation energies between 2 and 3.2 MeV (see text)

Transition	Pairing vibrations	Pairing rotations	Present experiment
$^{144}Nd(p,t)^{142}Nd_{gs}$	1	1	1.00
$^{146}Nd(p,t)^{144}Nd_{gs}$	2	1	1.22
$^{148}Nd(p,t)^{146}Nd_{gs}$	3	1	1.33
$^{142}Nd(p,t)^{140}Nd_{gs}$	1	1	0.90
$^{144}Nd(p,t)^{142}Nd_{pv}$	1	0	0.39(0.53)
$^{146}Nd(p,t)^{144}Nd_{pv}$	1	0	0.17(0.34)
$^{148}Nd(p,t)^{146}Nd_{pv}$	1	0	0.32(0.51)

limit, which is intermediate between the other two and the possibility to interpolate between different limits. In the intermediate case of transitional nuclei the system can be described in fact using parameters adjusted to obtain the observed excitation energies and transition probabilities. The parameters of the IBM-2 hamiltonian have been taken from the analysis performed by Scholten [18] on Sm, Gd and the heavier Nd isotopes (A = 146–152). These parameters have been extrapolated with quite good results [3] to reproduce inelastic scattering on ^{144}Nd. The model space of the present IBM analysis has been limited to valence particles outside the shell model closures at Z = 50 and N = 82. Within this space we cannot describe the closed-shell nucleus ^{142}Nd. The present IBM analysis is therefore limited to the $^{148,146}Nd(p,t)^{146,144}Nd$ reactions. The results of IBM calculations are given in Fig. 9 by crosses. The same normalization of the IBM strengths has been used for both reactions and has been chosen to reproduce at the best the transitions to the g.s. states in ^{144}Nd and ^{146}Nd. The agreement with 0_2^+ data is excellent: strengths and excitation energies in both nuclei are very well reproduced. No attempts have been made to improve the agreement for the transitions to higher-lying 0^+ states or to reproduce the transitions for other multipolarities, for which the situation is much more complex.

5. The quasi-particle phonon model

The quasi-particle phonon model (QPM) is based on the construction of a phonon basis, where the phonons are defined as solutions of the quasi-particle RPA equations. Starting from this basis, two- and multiple-phonon states are constructed (see for details Ref. [5]). The general hamiltonian of the QPM is usually written as

$$H = H_{sp} + H_{pair} + H_{ph}\,, \tag{1}$$

where $H_{\rm sp}$ is the single-particle part, the second term is the multipole separable pairing interaction:

$$H_{\rm pair} = -\frac{1}{4}\sum_{\tau} G_{\tau}^{(0)}(P_0^+ \cdot P_0)_{\tau} - \frac{1}{2}\sum_{\lambda>0,\tau} G_{\tau}^{(\lambda)}(P_{\lambda}^+ \cdot P_{\lambda})_{\tau},$$

$$P_{\lambda\mu}^+ = \sum_{jm,j'm'} (-1)^{j'-m'} \langle jm|i^{\lambda} f_{\lambda}(r) Y_{\lambda\mu}(\Omega)|j'm'\rangle a_{jm}^+ a_{j'm'}^+$$

and the third term is the p–h interaction:

$$H_{\rm ph} = -\frac{1}{2}\sum_{\lambda\mu,T} k_T^{(\lambda)}(M_{\lambda\mu}^+ \cdot M_{\lambda\mu})_T,$$

$$M_{\lambda\mu}^+ = \sum_{j,m,j',m'} \langle jm|i^{\lambda} f_{\lambda}(r) Y_{\lambda\mu}(\Omega)|j'm'\rangle a_{jm}^+ a_{j'm'},$$

where $f_{\lambda}(r)$ is the form factor of the separable residual interaction, $G_{\tau}^{(\lambda)}$ and $k_T^{(\lambda)}$ are the strengths in p–p and p–h channels, respectively. Protons and neutrons are indicated by τ, while isoscalar and isovector matrix elements by the isospin T. The form factor for $\lambda > 0$ was taken as the derivative dU/dr of the average field. A constant matrix element was used for the monopole pairing.

Phonons Q^+ are introduced as a linear combination of pairs of quasi-particle creation α^+ and annihilation α operators as follows:

$$Q_{\lambda\mu}^+(i) = \frac{1}{2}\sum_{\tau,j_1 j_2} \left(\psi_{j_1 j_2}^{\lambda i}\left[\alpha_{j_1}^+ \alpha_{j_2}^+\right]_{\lambda\mu} - (-1)^{\lambda-\mu}\phi_{j_1 j_2}^{\lambda i}\left[\alpha_{j_1}\alpha_{j_2}\right]_{\lambda-\mu}\right).$$

The reduced transition probability of the inelastic excitation of the one-phonon λ^{π} ith state from the ground state can be written [5] in terms of the forward $\psi_{j_1 j_2}^{\lambda i}$ and backward $\phi_{j_1 j_2}^{\lambda i}$ amplitudes of the phonon creation operator as

$$B(\mathrm{E}\lambda, \mathrm{g.s.} \rightarrow \lambda_i^{\pi}) = |M_i(\mathrm{E}\lambda)|^2$$

$$= \left|\sum_{\tau}^{N,Z} e_{\tau} \sum_{j_1 j_2} \frac{1}{2}\langle j_1||i^{\lambda} Y_{\lambda} r^{\lambda}||j_2\rangle \left(\psi_{j_1 j_2}^{\lambda i} + \phi_{j_1 j_2}^{\lambda i}\right)\left(u_{j_1} v_{j_2} + u_{j_2} v_{j_1}\right)\right|^2, \qquad (2)$$

where e_{τ} is an effective charge for neutrons and protons; u_j and v_j are Bogoliubov's coefficients of the transformation from particle a_{jm}^+ to quasi-particle α_{jm}^+ operators:

$$a_{jm}^+ = u_j \alpha_{jm}^+ + (-1)^{j-m} v_j \alpha_{j-m}.$$

The spectroscopic amplitude for the direct ${}^{A}\mathrm{X}(\mathrm{p,t})^{A-2}\mathrm{X}$ transition from the ground state of a (A)-nucleus to the $\{j_1 j_2\}_{\lambda}$ two-quasi-particle configuration of the one-phonon λ^{π} ith state of the $(A-2)$-nucleus has the form:

$$S(\mathrm{g.s.} \rightarrow \lambda_i^{\pi})_{j_1 j_2} = \frac{1}{\sqrt{1+\delta_{j_1,j_2}}} \prod_j \left(u_j^{(A-2)} u_j^{(A)} + v_j^{(A-2)} v_j^{(A)}\right)^{j+\frac{1}{2}}$$

$$\times \left[v_{j_1}^{(A-2)} v_{j_2}^{(A-2)} \psi_{j_1 j_2}^{\lambda i}(A-2) - u_{j_1}^{(A-2)} u_{j_2}^{(A-2)} \phi_{j_1 j_2}^{\lambda i}(A-2) \right]. \quad (3)$$

The term $\prod_j (u_j^{(A-2)} u_j^{(A)} + v_j^{(A-2)} v_j^{(A)})^{j+\frac{1}{2}}$ appears in this equation from the difference of the quasi-particle's vacuum in the (A) and $(A-2)$ systems. In our calculations it is equal to 0.53, 0.59, 0.89 and 0.92, respectively, for ^{140}Nd, ^{142}Nd, ^{144}Nd and ^{146}Nd as a residual nucleus.

In a second step of the QPM evaluations, one-, two- and three-phonon states are simultaneously coupled and mixed, i.e. we create a general space $\{\nu\}_\lambda$ from independent subspaces $\{i\}_\lambda$, $\{i_1 \times i_2\}_\lambda$, ...of one-, two-, ..., many-phonon configurations, respectively. Mixing of the subspaces is determined by diagonalizing the Hamiltonian of Eq. (1) with respect to the set of wave functions from the space $\{\nu\}_\lambda$. The equation for the spectroscopic amplitude is then transformed in

$$S(\text{g.s.} \rightarrow \lambda_\nu^\pi)_{j_1 j_2} = \sum_i R_i(\lambda\nu) S(g.s. \rightarrow \lambda_i^\pi)_{j_1 j_2}, \quad (4)$$

where $R_i(\lambda\nu)$ is the weight of the ith one-phonon component in the wave function of the νth state. The same equation is also valid for the amplitude of electromagnetic transitions M_ν by the substitution of $S(\text{g.s.} \rightarrow \lambda_i^\pi)_{j_1 j_2}$ by M_i in Eq. (4).

The differential cross section of the transition $A_{g.s.} \rightarrow (\text{A-2})_{\lambda_\nu^\pi}$ is obtained from a coherent sum of radial integrals of transition form factors, calculated with the codes DWUCK and CHUCK and weighted by the above QPM spectroscopic amplitudes. Because of the very high number of different neutron configurations, this type of calculation is time consuming. The comparison between calculations and data has been performed considering cross-section values at the maximum of the angular distributions. For this comparison a simplified procedure can be used. The cross section at the maximum can be calculated as

$$\sigma_{\max}(p,t) = N_t \left| \sum_{j_1 j_2} F_{j_1 j_2} S(\text{g.s.} \rightarrow \lambda_\nu^\pi)_{j_1 j_2} \right|^2, \quad (5)$$

where $F_{j_1 j_2}$ are coefficients proportional to the transition form factor at the nuclear surface or, more precisely, are the square roots of the cross section produced by the different $\{j_1 j_2\}$ configurations. To have the correct interference between different configurations, the sign of $F_{j_1 j_2}$ was taken equal to that of the transition form factor at the nuclear surface and at larger distances.

$B(\text{E}\lambda)$ values and cross sections, calculated with Eqs. (2)–(5), have been compared with the experimental $B(\text{E}\lambda)$'s and the (p,t) cross sections at the maximum of the angular distribution, obtained from the experimental data as described in Section 2. In these comparisons an important point is the capability of the model to reproduce the experimental spectra, that is to say the inelastic and (p,t) strength distributions. Another important point is connected with the absolute values of the observables considered. The uncertainties in the absolute normalization of the calculated σ(p,t) have been discussed in Section 3. A similar situation, connected to the effective charges used, is found in

calculating the $B(E\lambda)$ values from the QPM transition matrix elements. The effective charges compensate for the truncation of the basis states of the average field, namely in our case for the neglect of unbound states. For quite heavy nuclei, like Nd isotopes, and low-lying states one can expect the role of the continuum to be not very strong and thus, the continuum can be substituted by a limited number of quasi-bound states. This is the motivation in Refs. [19–21] for not using effective charges in the analysis of the transition densities in $^{142-146}$Nd. In the calculations of the strength distributions in ^{142,144,146}Nd we have found instead necessary [3] to use effective charges of the order of 1.2. The use of an effective pairing interaction leads to a larger value of the effective charge which should therefore be considered as an additional parameter in the present calculations.

6. Comparison with the experimental data

Recently QPM evaluations have been compared with inelastic scattering experiments on Nd isotopes: ^{142}Nd(e,e′) [19], ^{144}Nd(e,e′) [20], ^{146}Nd(e,e′) [21], (p,p′) and (d,d′) on ^{142,144,146,150}Nd [3]. Some of the assumptions used in these studies have been maintained also in the present calculations. The single-particle hamiltonian includes Saxon–Woods potentials with radial parameters taken as in the above references. All bound and narrow quasi-bound states were included in the calculation. In principle, for each multipolarity the parameters $k_{0,1}^{J^\pi}$ of the effective residual force can be chosen to reproduce the experimental excitation energy of the lowest state. To restrict the number of free parameters involved in the calculation the isovector constants have been fixed to the isoscalar ones by the following relation: $k_1^{J^\pi} = -1.2k_0^{J^\pi}$ for all J^π. A further constraint has been introduced for the higher multipolarities. Since our calculations indicate that the lowest states with $J \geqslant 5$ have strong components of multiphonon configurations, adjusting one-phonon parameters to the properties of these states is meaningless. Thus the value of $k_0^{5^-}$, for the 5^- states, was taken equal to that for the octupole states, i.e. equal to $k_0^{3^-}$, and that for 6^+ states to that for the quadrupole states, $k_0^{2^+}$.

The monopole pairing constant was fixed by the pairing energy. In Refs. [3,19–21] no other multipoles of the pairing interaction were considered. The experimental and the calculated $B(E2)$ and (p,t) cross sections for the excitation of the 2^+ states in ^{144}Nd are given in Fig. 10. The calculated strength distributions, obtained without quadrupole pairing ($G^{(2)} = 0$), have been normalized to the experimental ones assuming an effective charge $e = 1.3$ and a (p,t) normalization factor $N_t = 70$. The cross section for the excitation of the 2_1^+ state is underestimated by three order of magnitude with respect to the other states. The strength of this transition is expected to be strongly affected by pairing correlations and therefore by the pairing interaction. To explore this effect the parameter $G_\tau^{(2)}$ has been varied between 0 and 0.012. In these calculations equal values of $G_\tau^{(2)}$ and of the other $G_\tau^{(\lambda)}$ have been taken for protons and neutrons. The use of the pairing interaction also for $\lambda > 0$ produces a variation in the calculated excitation energies. The agreement with the experiment can be restored adjusting slightly

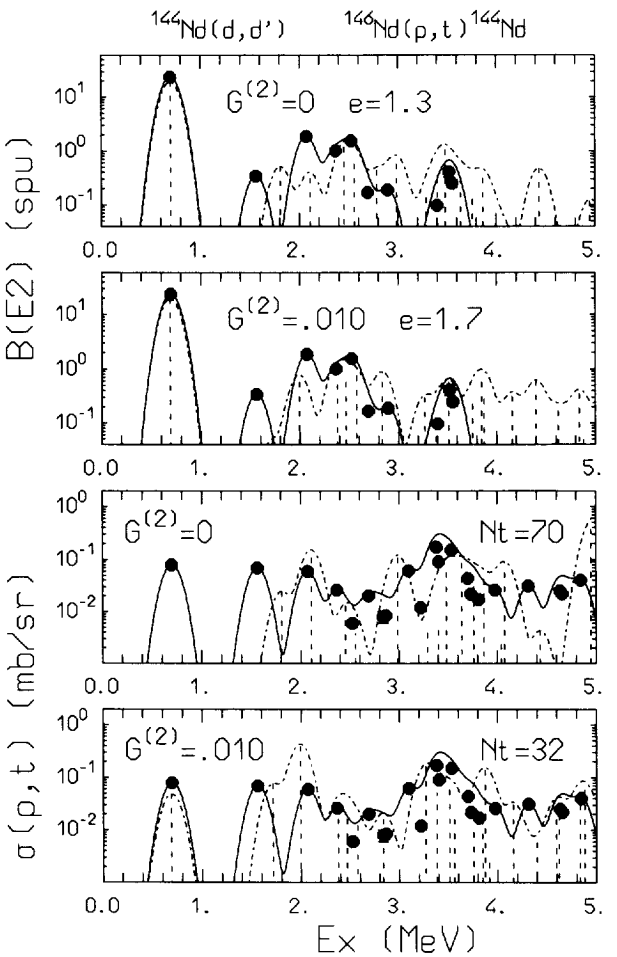

Fig. 10. Experimental transition probabilities, B(E2), and (p,t) cross sections at the maximum of the angular distribution (full points) leading to states in ^{144}Nd, compared with QPM evaluations (vertical dashed lines). To better appreciate the agreement in both the energy position and the strength value the data and the QPM evaluations are also presented as overlapping distributions after smearing with a 200 keV wide gaussian function (full and dashed curves, respectively). Values adopted for the quadrupole pairing interaction ($G^{(2)}$), the effective charge (e) and the empirical normalization factor (N_t) are given in each figure.

the multipole force in the p–h channel. For instance, in ^{144}Nd a variation in $G^{(\lambda)}$ from 0 to 0.010 leads to the following changes in the values of $k_0^{2^+}$, $k_0^{3^-}$, $k_0^{4^+}$: 0.0139→0.0125, 0.0126→0.0110, 0.0129→0.129 fm^2 MeV^{-1}, respectively. Similarly in ^{146}Nd the change is 0.0137→0.0120, 0.0123→0.0119, 0.0127→0.0124.

When a large quadrupole pairing interaction ($G^{(2)} = 0.01$) is considered, the agreement for the transition to the 2_1^+ state is strongly improved (Fig. 10). The B(E2) values are strongly reduced, causing an increase of the effective charge to $e = 1.7$. Moreover, the (p,t) cross sections are enhanced leading to a reduction of the N_t value to 32. In the case of ^{146}Nd, best fits to B(E2) and (p,t) data without the quadrupole pairing

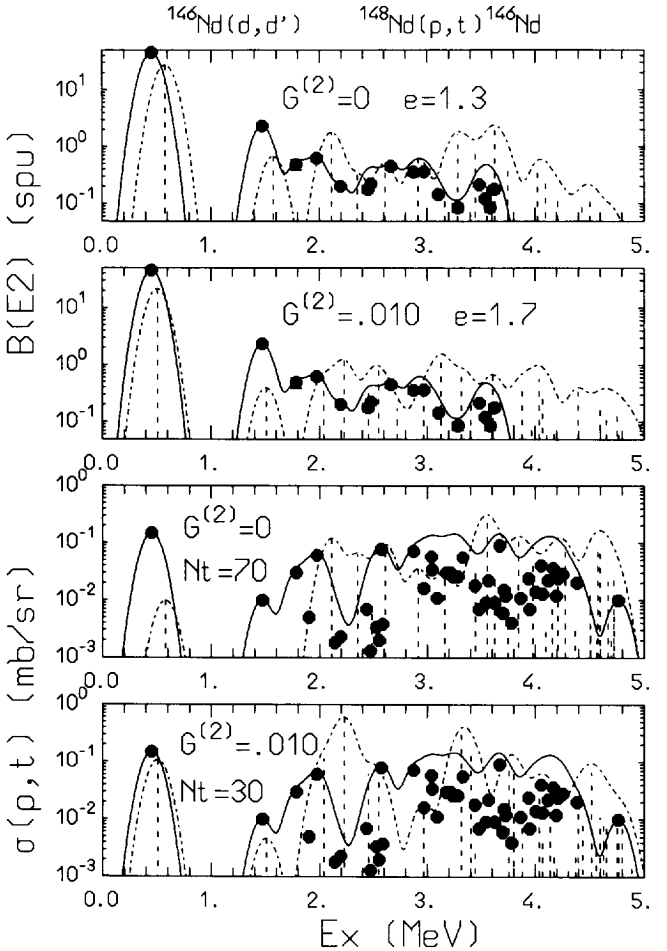

Fig. 11. As in Fig. 10 for transitions leading to 2^+ states in ^{146}Nd.

interaction are obtained with $e = 1.3$ and $N_t = 70$ (Fig. 11). The B(E2) values of the 2_1^+ and 2_2^+ states are underestimated with respect to those of higher-lying states. This problem was already found in a previous study [3] and was discussed in Ref. [21] in which the QPM transition charge densities were compared to experimental ones. It was concluded that the lowest 2^+ and 4^+ excited states in transitional ^{146}Nd display deformation effects while all other excited states could be treated reasonably well in the spherical approach. For this reason, as shown also in Fig. 12, it is not possible to reproduce the B(E2) value for the 2_1^+ state using the same $G^{(2)}$ and effective-charge values as for the other transitions. The (p,t) transitions to the three lowest 2^+ states are strongly underestimated. A better agreement for these transitions is found with $G^{(2)} \simeq 0.010$ and absolute normalizations $e = 1.7$ and $N_t = 30$.

For a more clear test of the $G^{(\lambda)}$ dependence, the strength of the 2_1^+ state and the summed strength of the other 2^+ states lying at low excitation energies ($\leqslant 3.8$ MeV)

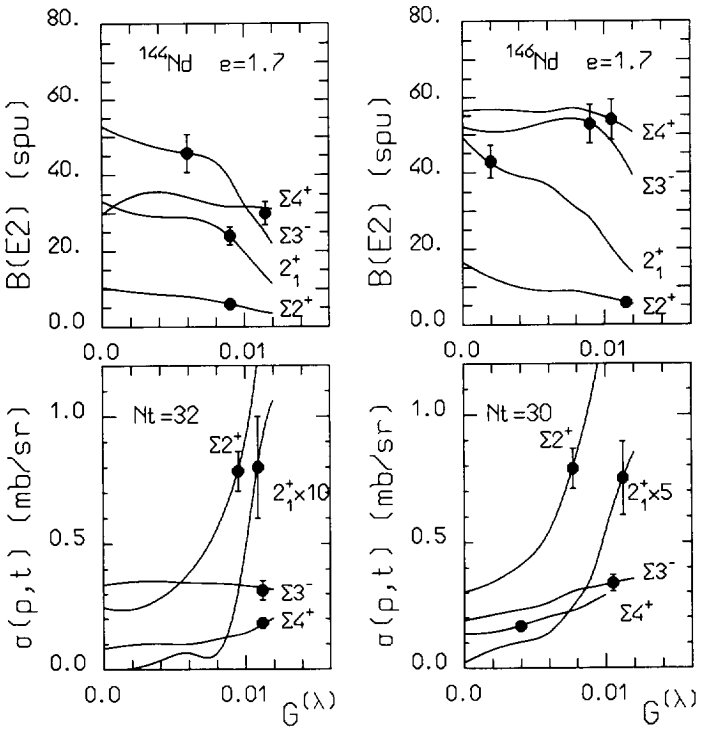

Fig. 12. $B(E\lambda)$ and σ(p,t) values for the first 2^+ state, the sum of the other 2^+ and of the 3^- and 4^+ states lying at excitation energies below 3.8 MeV. The full curves show the dependence of the QPM predictions on $G^{(\lambda)}$. The full points are ^{144}Nd and ^{146}Nd data. They are drawn on the QPM curves to have an indication of the $G^{(\lambda)}$ value needed to reproduce the different data. The polarization charges (e) and the normalization factors (N_t) are given.

are compared with calculations in Fig. 12. The $B(E2)$ value of the 2_1^+ state decreases by a factor larger than 2 in the explored $G^{(2)}$ range. The value of the summed $B(E2)$'s for the other 2^+ states is also strongly decreasing. A more complex but generally increasing trend is shown by the (p,t) cross sections. The effect is particularly evident, as expected, in the cross section for the excitation of the 2_1^+ state. The trends of $B(E2)$ and σ(p,t) would be interchanged in comparison to those shown in Fig. 12 by increasing the k_0^2 value at a fixed $G^{(2)}$ value. In the same figure the comparisons for the summed strengths of the transitions leading to the 3^- and 4^+ states are also shown. To have an indication of the $G^{(\lambda)}$ value needed to reproduce the different data, the experimental values are drawn on the QPM curves. The best overall agreement between calculation and data is obtained with a pairing interaction of the order of 0.010. It should be stressed that a satisfactory overall agreement is found using the same pairing interaction and very similar absolute normalizations for the transitions leading to the 2^+, 3^- and 4^- states in ^{144}Nd and ^{146}Nd. The agreement obtained in reproducing the 3^- and 4^+ (p,t) strengths is shown in Fig. 13 in the case of ^{144}Nd. The weaker $G^{(3)}$ dependence of QPM cross sections for the 3^- transitions (Figs. 12 and 13) leads to a N_t value of 32 also at

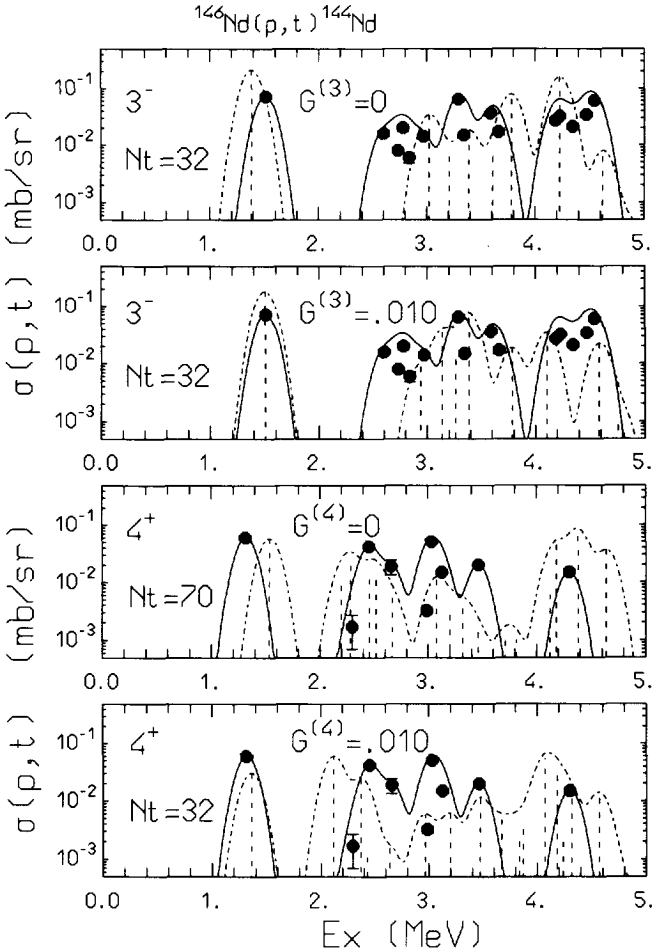

Fig. 13. As in Fig. 10 for (p,t) transitions leading to 3^- and 4^+ states in ^{144}Nd. It must be noticed that in the two upper figures, differently than for the other QPM calculations, the same N_t value has been assumed in calculating the QPM curves (see Section 7 and Fig. 12).

$G^{(3)} = 0$. This weaker dependence is discussed in Section 7.

No experimental data on the $B(E\lambda)$ strength distribution in the unstable ^{140}Nd are available. A comparison of the excitation of 2^+ states in the (p,t) reaction on this isotope with the results of QPM calculation is presented in Fig. 14. We leave a more detailed discussion to the next section and mention here only three major features. First, the 2_1^+ transition displays a strong direct component, it is to say a very large cross section without any evidence of two-step contributions, differently from the similar transitions in the other nuclei. A large direct component is also predicted by QPM calculations. Second, the dependence of the calculated cross section on the value of the residual pairing interaction is much weaker as compared to the two other isotopes. Third, the value of the normalization factor N_t is much smaller than in the case of ^{144,146}Nd, in

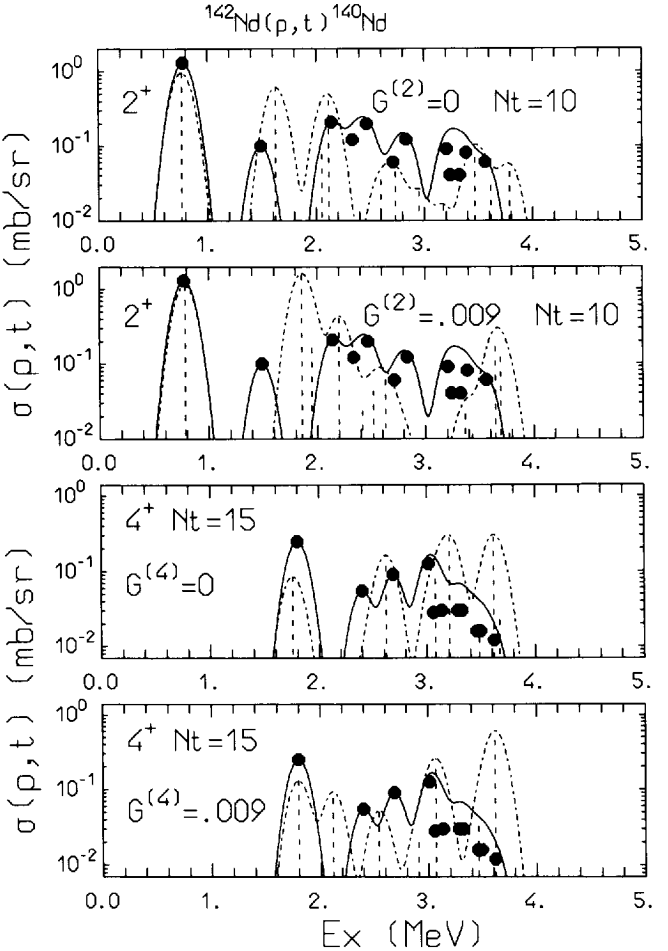

Fig. 14. As in Fig. 10 for (p,t) transitions leading to 2^+ and 4^+ states in ^{140}Nd.

spite of the larger ^{142}Nd(p,t)^{140}Nd cross sections.

7. Discussion

The p–h and pairing residual interactions are very important in determining energy spectra and strength distributions. The energy of the 2^+ state decreases from the two-quasi-particle energy to the experimental value increasing the value of k_0^2. At the same time the $B(\mathrm{E2})$ value increases. These effects are due to ground-state correlations generated by the p–h interaction. These correlations can be viewed microscopically as scattering of quasi-particles across the Fermi surface. The pairing interaction produces another type of correlations, which correspond to p–p and h–h type excitations and enhance the two-neutron transfer cross sections.

The most clear example of the role of the two parts of the residual interaction is found in closed-shell nuclei. The Bogoliubov's coefficients are $u_j = 0$ and $v_j = 1$ for the levels below the Fermi surface and vice versa for the levels above it. In this case the p–h and pairing channels of the residual interaction produce two different types of phonons. The p–h phonons, i.e. collective excitations created from p–h $\{j_1 j_2\}$ configurations, have non-vanishing $B(E\lambda)$ values since $u_{j_1} v_{j_2} = 1$ (see Eq. (2)) and give a zero value for the spectroscopic amplitude of the direct (p,t) reaction since $u_{j_1} u_{j_2} = v_{j_1} v_{j_2} = 0$ (see Eq. (3)). The h–h phonons, also often called removal-type vibrations, possess the reverse properties, since for h–h configurations $u_{j_1} v_{j_2} = 0$ and $v_{j_1} v_{j_2} = 1$. The present QPM calculations predict, therefore, that two completely different sets of levels should be populated by inelastic scattering and two-neutron transfer excitations. As mentioned in Section 2 the decoupling in ^{142}Nd is larger than in the other Nd isotopes, but is not complete. For this reason the results of ^{144}Nd(p,t)^{142}Nd evaluations are not presented here.

In nuclei with a developed pairing in the ground state these two sets of phonons are mixed in one set. Also the description of any two-quasi-particle configuration as p–h or h–h has no more a definite meaning. Each $\{jj'\}$ configuration can be considered as a p–h one with the probability $u_j v_{j'}$ and at the same time as h–h one with the probability $v_j v_{j'}$. In this situation the properties of excited states result from the interplay between two different parts of the residual interaction. The existence of p–h correlations blocks single-particle states which therefore cannot be used to generate h–h correlations and vice versa. The total amount of ground-state correlations is then a result of this interplay. A simple analysis of Eq. (3) shows that we have to expect different cross sections for the excitation of low-lying states in the ^{142}Nd(p,t)^{140}Nd and those in the ^{146,148}Nd(p,t)^{144,146}Nd reactions.

The position of the Fermi surface in the residual ^{144,146}Nd nuclei is close to that of the filling particle levels. Thus, the two-quasi-particle configurations, which give the main contribution to the structure of the lowest phonons, have the p–h nature with $v_j < u_j$. On the other hand, for phonon amplitudes we have $|\psi^{\lambda i}_{j_1 j_2}| > |\phi^{\lambda i}_{j_1 j_2}|$ and the same sign of $\psi^{\lambda i}_{j_1 j_2}$ and $\phi^{\lambda i}_{j_1 j_2}$ for the lowest collective phonon. This results in a strong compensation of two terms $v_{j_1} v_{j_2} \psi^{\lambda i}_{j_1 j_2}$ and $u_{j_1} u_{j_2} \phi^{\lambda i}_{j_1 j_2}$ of Eq. (3) for the main two-quasi-particle configurations in these isotopes and a weak (p,t) cross section at small $G^{(\lambda)}$ values. The h–h configurations which give rise to the (p,t) cross section are located a few MeV higher and one needs to increase sufficiently the residual pairing interaction to bring their strength down. This explains why the (p,t) cross section in these isotopes is very small at $G^{(2)} = 0$ and also why it strongly increases with an increase of the $G^{(2)}$ value. It can be remarked that the increasing trend of the (p,t) cross sections with $G^{(2)}$ is not due to the enhancement of the spectroscopic amplitude of specific configurations, which are instead decreasing as shown in Fig. 15, but to a more constructive interference between the contributions from the different configurations. The enhancement of (p,t) cross sections is therefore originating from a cooperative effect due to g.s. correlations and thus is analogous to that produced by p–h correlations in $B(E2)$ values. The best $G^{(2)}$ value 0.010 obtained in the present study is in good agreement with the value

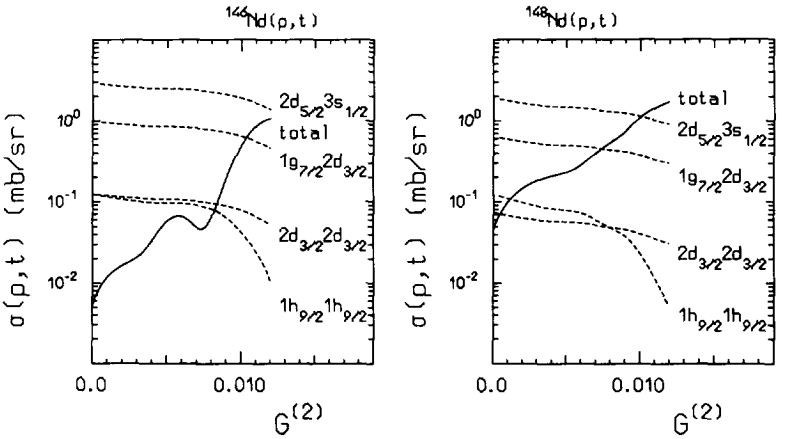

Fig. 15. Dependence of the ^{146,148}Nd(p,t) cross sections from the quadrupole pairing interaction $G^{(2)}$. The dashed curves represent contributions of specific two-neutron configurations (indicated in the figure); the full curves (indicated as "total") give the coherent sum of 105 different configurations.

estimated within the QPM by Soloviev and Sushkov [22] in the case of deformed nuclei: $G_0^{20} = 0.9k_0^{20} \simeq 0.011$.

The situation with other multipolarities is the following. The cross section of $\lambda^\pi = 4^+$ states reveals also an enhancement as a function of $G^{(4)}$ although weaker than for 2^+ states because of the lower collectivity of high multipolarity states. The lowest 3^- phonon states are constructed mainly of proton two-quasi-particle configurations, the leading one is $[2d_{5/2}1h_{11/2}]_\pi$. The interplay of p–h and pairing residual interactions in these configurations results in a (p,t) cross section which is practically constant as a function in $G^{(3)}$. On the other hand, an increase of $G^{(3)}$ corresponds to a larger contribution of the h–h proton channel in the 3^- phonon which reduces strongly the B(E3) value.

In the residual ^{140}Nd nucleus, the Fermi surface is located near the hole levels. The lowest phonons have mainly the h–h nature and the term $v_{j_1}v_{j_2}\psi^{\lambda i}_{j_1 j_2}$ in Eq. (3) strongly dominates the spectroscopic amplitudes of the main configurations. All this explains why the measured cross sections in ^{140}Nd are larger than in the ^{144,146}Nd isotopes. Moreover, the expected increase of the (p,t) cross section as a function of $G^{(\lambda)}$ is not evident anymore because of the presence of contributions of these main h–h configurations in the lowest phonons even at $G^{(\lambda)} = 0$. However, it seems that the QPM in the present form overestimates the contribution of the levels near the Fermi surface. This was noticed for the first time in comparing calculated transition charge densities with those extracted from (e,e′) scattering [19–21]. An overestimated contribution of the $(2d_{5/2},2d_{5/2})_\pi$ configuration to the structure of the first 2^+ and 4^+ states in the Nd chain resulted in a too large inner peak in the transition charge densities of these states. Similarly few two-quasi-particle configurations constructed with the $3s_{1/2}(\nu)$, $1h_{11/2}(\nu)$ and $2d_{3/2}(\nu)$ hole levels produce very large values of the spectroscopic amplitudes of the lowest phonons in ^{140}Nd. As a result the calculated values of the ^{142}Nd(p,t)^{140}Nd

cross sections are in general overestimated, i.e. we need to use a value of the empirical factor N_t about three times smaller than that used for the other Nd isotopes. This effect is not observed in ^{144,146}Nd because of the above mentioned cancellation. Collective observables like the $B(E\lambda)$ values, which are produced by a coherent contribution of many weak configurations, are not affected.

To improve the situation one has to take into account the ground-state correlations. The spectroscopic amplitude gets then an additional factor $(1 - q_{j_1} - q_{j_2})$, where q_j is the number of quasi-particles in the ground-state wave function. If the ground-state correlations are treated within the RPA as done by Rowe [23], the coefficients q_j can be calculated as

$$q_j = \frac{1}{2} \sum_{\lambda i j'} \frac{2\lambda + 1}{2j + 1} (\phi^{\lambda i}_{jj'})^2 .$$

Using this equation we obtained q_j values of only a few percent for the levels near the Fermi surface. Recently, Karadjov et al. [24] have calculated the coefficients q_j with the same hamiltonian (1) going beyond the RPA by solving a system of non-linear equations and obtained q_j values a few times larger. Unfortunately, taking into account consistently the ground-state correlations together with mixing to complex configurations creates serious technical problems which have not yet been solved. Summarizing, these corrections do not affect substantially the results in ^{144,146}Nd calculations and change those in ^{140}Nd in the right direction, but they are not sufficient to explain the N_t value found for ^{140}Nd with respect to that for ^{146}Nd and ^{148}Nd.

The calculated reduced probabilities, $B(E\lambda)$, and the (p,t) cross sections have relative values that look quite reasonable, as shown by the agreement with the experimental strength distributions (Figs. 10, 11 and 13). As described above, the agreement with (p,t) data has been obtained taking into account pairing correlations. We must however mention again that this procedure leads to the use of very large values of the effective charges in order to restore the agreement in the absolute values of $B(E\lambda)$'s. The reason is the following. Coupling one-phonon configurations to more complex ones results in a lowering of the energy of the lowest excited state from that of the first one-phonon configuration. This fact and the procedure we use in fitting the parameters of the residual interaction, i.e. to adjust the energy of the first excited state for each multipolarity at the experimental value, require energies of the first phonons a few hundred keV higher than the experimental ones. The collectivity of the lowest phonons under these conditions is underestimated. This effect becomes stronger when a larger two-phonon basis is used in the calculations. In previous calculations [3] a reasonable value of the effective charge was enough to compensate the effect. The coupling with complex one-phonon states produced by the residual pairing interaction moves a part of the phonon collectivity in the h–h and p–p channels, leaving the collectivity in the p–h channel strongly underestimated. At the same time, the ground state is considered as a phonon vacuum like in the one-phonon approximation. To improve this situation, one should take into account the influence of the phonon coupling on the ground-state wave functions.

8. Conclusions

The results of a (p,t) experiment on ^{142,144,146,148}Nd targets are presented and are analyzed together with inelastic proton and deuteron scattering data. Several new states have been detected and their spin-parity has been assigned. The (p,t) data for the excitation of the 0^+ states show that Nd isotopes constitute a transitional region from pairing vibrations to pairing rotations. Inelastic scattering and two-neutron transfer data have been used to estimate the strength of the residual pairing interaction in the quasi-particle-phonon model. The best overall description of the $B(E\lambda)$ and (p,t) strength distributions over the investigated energy region has been obtained with a strength of the particle–particle residual interaction close to the isoscalar strength in the particle–hole channel. Several shortcomings and limitations of the model have been evidenced. The directions in which this model should be developed have been pointed out. In particular a better description of ground-state wave functions is clearly needed.

Acknowledgements

The authors are indebted to Ricardo Broglia for several discussions and comments. V.Yu.P. thanks the Dipartimento di Fisica of the Università di Milano for the hospitality and acknowledges a financial support from the INFN, the International Science Foundation under the grant N6N000 and the RFFI under the grant 95-02-05701. Part of this work was performed within the research program of the Stichting voor Fundamenteel Onderzoek der Materie (FOM) with financial support of the Nederlandse Organisatie voor Wetenchappelijk Onderzoek (NWO).

References

[1] A. Bohr, in Nuclear Structure, Dubna Symp., IAEA, Vienna (Benjamin, Reading, MA, 1968) p. 179.
[2] R.A. Broglia, O. Hansen and C. Riedel, Adv. Nucl. Phys. 6 (1973) 287;
D.R. Bes, R.A. Broglia, O. Hansen and O. Nathan, Phys. Reports C 34 (1977) 1.
[3] M. Pignanelli, N. Blasi, J.A. Bordewijk, R. De Leo, M.N. Harakeh, M.A. Hofstee, S. Micheletti, R. Perrino, V.Yu. Ponomarev, V.G. Soloviev, A.V. Sushkov and S.Y. van der Werf, Nucl. Phys. A 559 (1993) 1.
[4] A. Arima and F. Iachello, Ann. Phys. 111 (1978) 201.
[5] V.G. Soloviev, Z. Phys. A 334 (1989) 143;
A.I. Vdovin and V.G. Soloviev, Sov. J. Part. Nucl. 14 (1983) 99;
V.V. Voronov and V.G. Soloviev, Sov. J. Part. Nucl. 14 (1983) 583.
[6] J.B. Ball, R.L. Auble, J. Rapaport and C.B. Fulmer, Phys. Lett. B 30 (1969) 533.
[7] K. Yagi, Y. Aoki, J. Kawa and K. Sato, Phys. Lett. B 29 (1969) 647;
K. Yagi, K. Sato, Y. Aoki, T. Udagawa and T. Tamura, Phys. Rev. Lett. 29 (1972) 1334.
[8] L.K. Peker, Nucl. Data Sheets 51 (1987) 425.
[9] L.K. Peker, Nucl. Data Sheets 63 (1991) 474.
[10] J.K. Tuli, Nucl. Data Sheets 56 (1989) 607.
[11] L.K. Peker, Nucl. Data Sheets 60 (1990) 953.
[12] J. Kern, Phys. Lett. B 320 (1994) 7.
[13] P.D. Kunz, Computer codes DWUCK 4 and CHUCK, Univ. of Colorado, unpublished.

[14] F.D. Becchetti and G.W. Greenlees, Phys. Rev. 182 (1969) 1190.
[15] R.J. Ascuitto, N.K. Glendenning and B. Sorensen, Nucl. Phys. A 183 (1972) 60.
[16] M. Igarashi, K. Kubo and K. Yagi, Phys. Reports 1 (1991) 1.
[17] L. Trache, C. Wesselborg, P. von Brentano, J. Wrzesinski and G.P.A. Berg, Nucl. Phys. A 540 (1992) 66.
[18] O. Scholten, Ph.D. Thesis, University of Groningen (1980); the programs NPBOS and NPTPT, KVI internal report 253 (1979).
[19] R.K.J. Sandor, H.P. Blok, U. Garg, M.N. Harakeh, C.W. de Jager, V.Yu. Ponomarev, A.I. Vdovin and H. de Vries, Nucl. Phys. A 535 (1991) 669.
[20] R. Perrino, N. Blasi, R. De Leo, M.N. Harakeh, C.W. de Jager, S. Micheletti, J. Mieremet, M. Pignanelli, V.Yu. Ponomarev, R.K.J. Sandor and H. de Vries, Nucl. Phys. A 561 (1993) 343.
[21] R.K.J. Sandor, H.P. Blok, M. Girod, M.N. Harakeh, C.W. de Jager, V.Yu. Ponomarev and H. de Vries, Nucl. Phys. A 551 (1993) 378.
[22] V.G. Soloviev and A.V. Sushkov, Z. Phys. A 345 (1993) 155.
[23] D.J. Rowe, Phys. Rev. 175 (1968) 1283.
[24] D. Karadjov, V.V. Voronov and F. Catara, Phys. Lett. B 306 (1993) 197; J. Phys. G 20 (1994) 1431.